Journal of Mathematical Biology (2026) 93:13
https://doi.org/10.1007/s00285-026-02423-0

Mathematical Biology

A perception-memory PDE framework for seasonal migration dynamics

Qi An[1,2] · Xiunan Wang[3] · Pinar Baydemir[4,5] · William F. Fagan[4] · Peng Wu[6] · Briana Abrahms[7] · Hao Wang[8]

Received: 22 November 2025 / Revised: 14 April 2026 / Accepted: 1 June 2026

Abstract

Seasonally migrating animals must navigate environments where resources shift predictably but are increasingly perturbed by climate change and human activities. Empirical work highlights the importance of cognition for these movements, yet the joint roles of perception and memory in sustaining stable seasonal migration remain poorly understood. We develop and analyze a novel PDE (partial differential equation) model that couples random dispersal with two taxis processes: perception-driven movement toward a nonlocally sensed, periodically shifting resource, and memory-driven movement guided by a spatiotemporal map of past foraging successes over seasonal time windows. We first establish global well-posedness of the system, proving existence, uniqueness, and uniform boundedness of classical solutions. Using Leray-Schauder degree theory, we then show that the model admits at least one

Qi An and Xiunan Wang contributed equally to this work.

✉ Hao Wang
hao8@ualberta.ca

1 Department of Mathematics, Nanjing University of Information Science and Technology, Nanjing 210044, P.R. China

2 Jiangsu International Joint Laboratory on System Modeling and Data Analysis & Center for Applied Mathematics of Jiangsu Province, Nanjing University of Information Science and Technology, Nanjing, China

3 Department of Mathematics, University of Tennessee at Chattanooga, Chattanooga, TN 37403, USA

4 Department of Biology, University of Maryland, College Park, MD, USA

5 Department of Mathematics, TOBB University of Economics and Technology, 06510 Ankara, Türkiye

6 School of Sciences, Hangzhou Dianzi University, Hangzhou 310018, China

7 Department of Biology, Center for Ecosystem Sentinels, University of Washington, Seattle, WA, USA

8 Department of Mathematical and Statistical Sciences, University of Alberta, Edmonton, AB T6G2G1, Canada

Published online: 04 July 2026

time-periodic solution synchronized with the seasonal resource. By constructing a Lyapunov-Krasovskii functional, we further derive sufficient conditions under which this periodic migratory pattern is unique and globally asymptotically stable, revealing a key trade-off between perception- and memory-driven taxis strengths and diffusive spreading. Numerical simulations corroborate the analytical results and demonstrate how the balance of perception and memory, the precision of memory, and its match or mismatch with environmental periodicity jointly govern migration efficiency and persistence. Together, these results provide a rigorous theoretical framework linking individual-level cognitive processes to the emergence, stability, and breakdown of seasonal migration routes in changing environments.

Keywords Cognitive movement ecology · Seasonal migration · Nonlocal perception · Memory-driven movement · Periodic solutions · Global stability

Mathematics Subject Classification 35B99 · 35B10 · 92-10

1 Introduction

Seasonal migration is a remarkable and widespread ecological phenomenon, driving vast animal populations to undertake regular, long-distance movements between distinct geographical regions (Dingle 2014; Milner-Gulland and Fryxell 2011). These migrations are primarily motivated by the pursuit of favorable foraging opportunities, optimal breeding conditions, or the avoidance of harsh environmental factors such as extreme temperatures or elevated predation risk (Alerstam et al. 2003; Somveille et al. 2013). Terrestrial ungulates, insectivorous birds, and cetaceans are among the many kinds of migratory species that traverse dynamic environments in which resources fluctuate (roughly) predictably in both space and time (Dingle 2014). Such large-scale movements are not solely governed by immediate environmental cues; rather, they often depend on complex cognitive processes involving memory, learning, and perception (Bracis and Mueller 2017). Instead of responding only to nonlocal resource gradients, migrating individuals frequently draw upon memory of past foraging success, recalling when and where resources were previously abundant. This stored knowledge is integrated with current perception, allowing animals to adjust their movement strategies according to both present signals and historically profitable locations. Through this combination of perception and memory, animals can track shifting resource patches across seasons, return to high-quality habitats, and maintain efficient migratory routes in environments that exhibit recurrent yet variable patterns of resource availability (Jerod et al. 2019; Bauer et al. 2020).

The interplay between perception and memory represents a key ecological trade-off. Perception enables animals to respond rapidly to immediate environmental changes, which can be advantageous in highly dynamic or unpredictable conditions (Mueller and William F Fagan 2008; Bradshaw and Holzapfel 2010). Memory, on the other hand, provides a means of exploiting past experience, offering benefits in more stable or cyclically varying environments (Mueller and William F Fagan 2008; Fagan et al. 2013). Over-reliance on either mechanism can be costly—depending too much

on perception may cause individuals to overlook predictable seasonal opportunities, while relying excessively on outdated memory can lead to inefficient or mistimed foraging. Memory is also inherently imperfect, often characterized by limited resolution or "fuzziness" in spatial and temporal recall (Shankar and Howard 2013). Such imperfect memory can in fact be adaptive, allowing animals to remain flexible and avoid rigid adherence to outdated information when environments change unexpectedly. Balancing perception, memory, and the uncertainty associated with past information is therefore critical for optimizing migratory decisions and maximizing long-term fitness.

Understanding how animals integrate perception and memory to guide seasonal migration has become a central theme in cognitive movement ecology(Gurarie and Avgar 2024). Moreover, this understanding has critical implications for conservation and climate adaptation (Fagan et al. 2013; Bracis and Mueller 2017). As global warming, altered precipitation regimes, and shifting ocean currents modify the timing, distribution, and abundance of resources, traditional migratory routes may no longer align with good foraging opportunities. Models that capture the cognitive mechanisms underlying animal movement can help predict how species will adjust their routes, expand or contract their ranges, and respond to emerging environmental challenges. Such insights are vital for identifying species at risk, designing effective protected areas, and implementing management strategies that sustain wildlife persistence in rapidly changing ecosystems.

Recent work on blue whales in the eastern North Pacific provides a compelling example. Using satellite tracking data combined with remotely sensed ocean productivity, Abrahms et al. (2019) demonstrated that migrating blue whales in this system do not primarily follow contemporaneous resource gradients, but instead align their migratory movements to when and where resources have been consistently reliable over many years. The whales' movements aligned with long-term averages in chlorophyll-a concentration—a proxy for the availability of krill, shrimp-like organisms that constitute their primary prey—rather than with the localized peaks in productivity that shifted from year to year. This finding indicates that blue whale foraging migration is memory-based: individuals rely on stored information about past resource locations to time and route their seasonal movement, rather than "surfing" present-day resource waves. This result has been highlighted as evidence that migratory success can depend on the ability to remember resource landscapes across large spatial and temporal scales, underscoring the importance of memory as a navigation mechanism in marine environments (Fagan 2019) as it is for some land-dwelling species like elephants (Polansky et al. 2015). This study of blue whales motivates the development of mathematical models that can represent how animals integrate memory and perception to guide seasonal migration. In particular, it raises fundamental questions about how memory forms, how it decays, how it interacts with real-time perception, and how these cognitive processes influence movement in environments where resources are seasonal and spatially shifting.

Advances in movement ecology have seen the development of specialized models to unravel the cognitive underpinnings of seasonal migration. Gurarie et al. (2021) developed a population-level partial differential equation (PDE) model that integrates diffusion, resource-following taxis, social swarming, and a memory-driven advection

term. Their model quantitatively demonstrates how a balance between long-term reference memory and short-term working memory, coupled with an optimal spatial scale of sociality, can foster resilient migratory behavior capable of adapting to directional environmental change and stochasticity. Complementing this macroscopic approach, Lin et al. (2021) proposed an individual-based model formulated via a stochastic differential equation coupled with an eikonal equation, where movement decisions are informed by a cognitive map built from multiple memory channels. They found that the interplay between long-term and short-term memory with appropriate time scales is crucial for generating stable periodic migrations in a dynamic environment, highlighting the importance of individual cognition. Further bridging the gap between theory and data, Peter R Thompson et al. (2022) introduced a statistical movement model embedded within a hidden Markov framework to detect seasonal, episodic-like spatiotemporal memory patterns directly from animal tracking data. Their method, which was demonstrated for grizzly bears, infers the characteristic time lag and precision of an animal's recursions to previously visited, resource-rich locations, providing a powerful tool for empirical validation of memory use in wild populations. Collectively, these works establish a theoretical foundation showing that memory is not merely a facilitator but a fundamental component enabling adaptive and plastic migratory strategies in dynamic seasonal environments.

While these and other studies have established the importance of memory in seasonal migration, crucial gaps remain in developing a unified PDE framework that directly couples dynamic internal memory states with externally forced seasonal environments at the population level, and in providing a comprehensive qualitative analysis of the resulting PDE dynamics. Both Othmer and Stevens (1997) and Howard et al. (1997) approach memory in movement processes by deriving continuum PDE models from reinforced random walks, in which past movement modifies future behavior. In these models, individuals deposit or respond to a non-diffusible signal that records aspects of prior passages, thereby introducing a form of environmental memory into the movement rules. Recent advances in PDE models have sought to move beyond simple random walks to capture the cognitive processes underlying animal movement, particularly through the incorporation of nonlocal perception and memory. For instance, several studies introduce "memory-based diffusion" via delay terms derived from modified Fickian laws, contrasting the directed movement of "clever" animals with the random dispersal of "drunk" particles (see, e.g., Shi et al. (2019, 2020); Song et al. (2019)). These models have revealed that the interplay between memory delays, nonlocal resource interactions, and standard diffusion can give rise to rich spatiotemporal dynamics, including Turing patterns, Hopf bifurcations, and the coexistence of multiple stable states. However, most of these PDE formulations treat memory as a uniformly decaying process, overlooking how seasonal patterns or distinct ecological events can shape the strength and persistence of memory. Integrating both memory effects and seasonal variability into a unified modeling framework remains challenging, as it requires representing the complex interactions between cognitive mechanisms and external environmental cues. Consequently, there is a pressing need for a PDE framework that combines nonlocal perception and memory dynamics with explicit periodic environmental forcing to describe seasonal cognitive migration—

anticipatory, large-scale animal movements that are tuned to predictable resource cycles.

Our work aims to bridge these gaps by developing and rigorously analyzing a novel PDE model that explicitly incorporates animal cognitive abilities to study seasonal, round-trip migrations, as observed in species such as cetaceans, ungulates, and birds. The model couples perception-driven movement with a dynamically evolving memory field in a seasonally shifting resource landscape, allowing us to directly investigate how the precision, accumulation, and decay of foraging memory interact with nonlocal perception to facilitate or hinder the emergence of resilient seasonal migratory patterns. Using this model, we investigate stable time-periodic solutions corresponding to round-trip seasonal migrations, and examine the interacting effects of perception and memory on emergent seasonal migration patterns. This study provides a unified framework for understanding how the integration of perception and memory underpins large-scale seasonal migrations in dynamic environments.

The remainder of this paper proceeds as follows. In Sect. 2, we formulate the mathematical model. We establish fundamental analytical results in Sect. 3, including the local existence of solutions, a blow-up criterion, and the global existence of solutions via *a priori* estimates. Sect. 4 characterizes the model's long-term dynamics by proving the existence, uniqueness and stability of time-periodic solutions. We support these analytical insights and explore the roles of perception and memory in seasonal migration with numerical simulations in Sect. 5 and conclude with a discussion of the ecological implications and future research directions in Sect. 6.

2 Model formulation

The model comprises two principal variables: the animal population density distribution $u(x,t)$ and a cognitive map of past foraging experiences as memory $m(x,t)$. We use the function $h(x,t)$ to represent the nonlocal perception of the resource density distribution $r(x,t)$. This distribution not only determines the perception-driven advection movement, but also influences the formation of memory and memory-driven advection movement, as it appears explicitly and implicitly in the right-hand-side terms of the model. The governing equations for our cognitive seasonal migration model are formulated as follows:

$$\begin{cases} \dfrac{\partial u}{\partial t} = d\dfrac{\partial^2 u}{\partial x^2} - \alpha\dfrac{\partial}{\partial x}\left(u\dfrac{\partial h}{\partial x}\right) - \gamma\dfrac{\partial}{\partial x}\left(u\dfrac{\partial}{\partial x}\displaystyle\int_\Omega m(y,t)J_p(x-y,R_J)\,dy\right), & x\in\Omega,\ t>0,\\ \dfrac{\partial m}{\partial t} = \varepsilon\dfrac{\partial^2 m}{\partial x^2} + \dfrac{1}{N}\displaystyle\sum_{i=1}^{N}\rho_i u(x,t-i\tau)h(x,t-i\tau) - \mu_m m, & x\in\Omega,\ t>0,\\ h(x,t) = \displaystyle\int_\Omega r(y,t)G_p(x-y,R_G)\,dy, & x\in\Omega,\ t>0, \end{cases} \tag{2.1}$$

for $\Omega = [0, L]$, and subject to periodic boundary conditions:

$$u(0,t) = u(L,t), \quad \frac{\partial u}{\partial x}(0,t) = \frac{\partial u}{\partial x}(L,t),$$

$$m(0,t) = m(L,t), \quad \frac{\partial m}{\partial x}(0,t) = \frac{\partial m}{\partial x}(L,t).$$

We now provide a detailed explanation of each component of the model (2.1). A comprehensive summary of all variables and parameters is provided in Table 1 for easy reference.

1. Animal distribution dynamics $u(x,t)$: The spatio-temporal dynamics of the animal population density $u(x,t)$ are governed by the first equation of system (2.1), which combines random dispersal with directed, adaptive movement. The term $d\frac{\partial^2 u}{\partial x^2}$ represents standard Fickian diffusion, where $d > 0$ quantifies the rate of undirected, random movement. Beyond diffusion, movement is guided by two primary taxis mechanisms that drive migration in response to a dynamic environment.

First, the term $-\alpha\frac{\partial}{\partial x}\left(u\frac{\partial h}{\partial x}\right)$ models taxis along gradients of perceived resource abundance, a standard formulation in mathematical ecology for chemotaxis and other gradient-following behaviors (Fagan et al. 2017, 2022). This formulation reflects the principle that it is the dynamic, rather than static, nature of resource distributions that fundamentally drives migration. The function $h(x,t)$ denotes the population's non-local perception of the actual resource quantity $r(x,t)$, enabling the tracking of seasonally shifting foraging opportunities.

Second, the term $-\gamma\frac{\partial}{\partial x}\left(u\frac{\partial}{\partial x}\int_\Omega m(y,t)J_p(x-y;R_J)\,dy\right)$ captures nonlocal advection influenced by the cognitive map, which can represent effects of both memory and social information (Gurarie et al. 2021; Fagan et al. 2013). This formulation reflects the sophisticated foraging strategies of many species (e.g., cetaceans), which may involve communication or other mechanisms for acquiring information beyond their immediate sensory range (Martínez-García et al. 2013; Hessing et al. 2024; Dodson et al. 2024). It embodies the hypothesis that animals can detect the non-local distribution of conspecifics, effectively sharing information about historically favorable or currently occupied areas (Martínez-García et al. 2013; Alcázar-Treviño et al. 1942). The parameter γ regulates the strength of taxis guided by the cognitive map. This directs movement along gradients of a "memory-informed landscape" derived from $m(x,t)$ via the interaction kernel J_p. This term can thus represent movement toward remembered foraging hotspots. Our model formulates this cognitive map $m(x,t)$ as a form of spatial memory, built from a history of past foraging experiences. However, the resulting dynamic can also be interpreted more broadly as a response to social cues, particularly if those cues themselves reflect the accumulated knowledge of the group. The specific forms of $r(x,t)$ and J_p are detailed below.

It is important to note that model (2.1) focuses on the spatial distribution of the population, rather than its demographic dynamics. As such, there are no reaction kinetics; the model does not include birth or death processes. This is reflected in the structure of the population equation, where all terms involve spatial derivatives, signifying that the equation only moves animals around the landscape. This formulation allows us to isolate and study the central question of how a migratory population matches, or fails to match, the spatio-temporal dynamics of the resource landscape through which it is moving. Furthermore, we assume that there is no explicit consumption of the resource, meaning there is no feedback from the migratory species onto the resource distribution itself. This assumption is biologically reasonable for scenarios where the

Table 1 Summary of model variables, parameters, and functions

Symbol	Description	Category
$u(x,t)$	Density of the migrating population.	State Variable
$m(x,t)$	Density of the cognitive memory map.	State Variable
α	Strength of perception-driven taxis.	Cognitive Parameter
γ	Strength of memory-guided taxis.	Cognitive Parameter
ε	Memory diffusion (controls spatial precision).	Cognitive Parameter
μ_m	Memory decay rate (forgetting).	Cognitive Parameter
τ	Duration of one historical memory window.	Cognitive Parameter
N	Number of historical memory windows.	Cognitive Parameter
ρ_i	Weights of historical memory in the i-th past year.	Cognitive Parameter
d	Population diffusion (random dispersal).	Movement Parameter
L	Length of the spatial domain Ω.	Domain Parameter
$r(x,t)$	Periodically shifting resource distribution.	External Forcing
$h(x,t)$	Perceived resource landscape.	Intermediate Function
A_r	Amplitude of the resource peak.	Resource Parameter
σ_r	Width of the resource.	Resource Parameter
T	Temporal period of the resource's movement.	Resource Parameter
$G_p(z; R_G)$	Perceptual kernel with range R_G.	Kernel Function
$J_p(z; R_J)$	Memory interaction kernel with range R_J.	Kernel Function

migratory population has a negligible impact on the vast resource base, a modeling choice also employed in other studies of large-scale movement (Turchin 1998; Fagan et al. 2013, 2022). In essence, this paper is about the cognitive strategies involved in tracking and matching a dynamic environment.

2. Memory dynamics $m(x,t)$: The cognitive map $m(x,t)$ evolves according to the second equation of system (2.1), shaped by processes of formation, decay, and spatial generalization. Memory formation is represented by the term $\frac{1}{N}\sum_{i=1}^{N}\rho_i u(x,t-i\tau)h(x,t-i\tau)$, which constitutes a weighted average of past foraging successes, with weights $\rho_i \geq 0$ describing the level of contribution of memory from the i-th past year. These foraging successes are modeled as the product (i.e., coincidence) of the population density u and the perceived resource abundance h over N discrete historical time windows (e.g., years). The duration τ represents the length of a memory window that is expected to equal the period of the seasonally emerging resource so that $t-i\tau$ depicts the same time point (e.g., date) in the i-th past year. The special case $i=0$ corresponds to the current year.

Concurrent with its formation, memory naturally decays at a rate of $\mu_m > 0$ via the term $-\mu_m m$, representing the process of forgetting. A key cognitive feature of our model is the inclusion of the term $\varepsilon\frac{\partial^2 m}{\partial x^2}$ for a positive ε, which models the spatial smoothing or diffusion of memories. This term is biologically justified as it represents the inherent imprecision in spatial recall—a process that can encompass both the generalization of learned information to nearby areas and random errors in recollection. By ensuring that remembered locations are approximate rather than exact point locations, this diffusion of memory provides a mathematically novel and clear mechanism to capture the fuzzy nature of cognitive maps (Gurarie et al. 2021). This entire formulation of memory dynamics draws on studies highlighting how accumulated experiences shape an organism's ecological understanding and subsequent behavioral decisions (Fagan et al. 2022; Potts and Lewis 2019).

3. Nonlocal resource perception $h(x,t)$: The function $h(x,t)$, defined by the third line in system (2.1), quantifies how animals perceive the contemporaneous abundance of the resource, $r(y,t)$. This perception is modeled as a nonlocal convolution:

$$h(x,t)=\int_{\Omega} r(y,t)G_p(x-y;R_G)\,dy. \tag{2.2}$$

This integral represents a spatially weighted average of the resource quantity $r(y,t)$ in the vicinity of location x. The weighting is given by the perceptual kernel G_p, which is characterized by the perceptual range R_G. This parameter specifies the spatial scale over which an animal integrates information about resource availability to form its perceived landscape of resource abundance, $h(x,t)$.

It is worth noting that both the perception-driven and memory-driven taxis mechanisms in our model are rooted in nonlocal perception. The perception-driven taxis is explicitly governed by the animal's current nonlocal perception of the surrounding resource landscape. In contrast, the memory-driven taxis does not rely on instantaneous perception but rather on the accumulated memory of past nonlocal perceptions over previous seasonal windows. In this sense, memory-driven movement integrates

historical sensory information to guide present behavior, reflecting how animals may recall and respond to previously experienced resource distributions.

4. Domain and boundary conditions: We consider the model on the one-dimensional spatial domain $\Omega = [0, L]$ with periodic boundary conditions. While this domain is topologically equivalent to a boundary-less 1D torus ($\mathbb{T} = \mathbb{R}/L\mathbb{Z}$), we formulate and analyze the model by unwrapping it onto the compact interval $\bar{\Omega} = [0, L]$. This standard PDE representation facilitates the rigorous definition of Hölder spaces and integral operators in our mathematical analysis. Furthermore, from an ecological perspective, this unrolled representation provides a clear geographic coordinate system for interpreting migratory dynamics. This gives a continuous, cyclical migratory habitat in which $x = 0$ and $x = L$ represent the same physical location in the real world. Take blue whales' seasonal migration as an example. The locations $x = 0$ and $x = L$ may represent the winter/breeding grounds in the Gulf of California or the Costa Rica Dome, while $x = L/2$ corresponds to the productive summer/foraging grounds at higher latitudes in the California Current (Helen et al. 2009; Ladd et al. 2014; Ballance et al. 2006; Mate et al. 1999). Each year, blue whales migrate from the winter/breeding grounds ($x = 0$) to the summer/foraging grounds at higher latitudes ($x = L/2$), and then return to the winter/breeding grounds ($x = L$). This migratory cycle repeats annually. Such a looped domain provides a natural and powerful simplification for many real-world seasonal migrations that follow closed, recurring circuits, such as the annual circuits of terrestrial ungulates or the oceanic pathways within pelagic gyres (Avgar et al. 2014). The 1D approximation is particularly reasonable for species that follow well-defined, narrow corridors where movement is predominantly along a single axis. Periodic boundaries are ideal for modeling these recurrent movements, eliminating artificial edge effects and enabling the use of analytical tools such as Fourier analysis for stability and pattern-formation studies (José et al. 2024; Murray 2002).

5. External resource distribution $r(x, t)$: The primary resource distribution $r(x, t)$, which drives the seasonal migration, is modeled as a traveling Gaussian peak whose center $x_0(t)$ executes a periodic round-trip across the domain Ω with period T (typically one year):

$$x_0(t) = \frac{L}{2}\left(1 - \cos\left(\frac{\pi t}{T}\right)\right). \tag{2.3}$$

At $t = 0$, the resource peak is centered at $x = 0$; it reaches the midpoint $x = L/2$ at $t = T/2$, and arrives at $x = L$ at the end of the seasonal cycle, $t = T$. The periodized resource distribution is then defined as:

$$r(x, t) = \sum_{k=-\infty}^{\infty} A_r \exp\left(-\frac{(x - x_0(t) + kL)^2}{2\sigma_r^2}\right), \tag{2.4}$$

where A_r is the resource amplitude and σ_r the spatial width. This formulation is designed to capture a seasonally shifting zone of high resource availability. The concept of animals tracking such a moving resource pulse is central to ideas like the "green wave" hypothesis, which posits that herbivores migrate to follow the wave of emerging, high-quality forage across a landscape (Merkle et al. 2016; Fagan et al. 2017; Ellen

et al. 2017). While our model simplifies the resource dynamics to a wave of pure quantity, the fundamental principle of a moving target driving migration is the same.

6. Kernel functions G_p and J_p: The nonlocal interactions in the model are mediated by kernel functions. These kernels define how the influence of a resource or memory at one location decays with spatial distance. Both the perceptual kernel G_p and the memory-based interaction kernel J_p are modeled as periodized Gaussian functions to ensure consistency with the periodic domain. The general form is a function of the spatial displacement, $z = x - y$. A standard Gaussian is periodized by summing over all its periodic images, which are centered at integer multiples of the domain length, kL, for $k \in \mathbb{Z}$:

$$K_p(z; R_K) = \sum_{k=-\infty}^{\infty} \frac{1}{\sqrt{2\pi} R_K} \exp\left(-\frac{(z - kL)^2}{2R_K^2}\right), \tag{2.5}$$

where K_p represents either G_p or J_p, and R_K denotes the respective spatial scale (R_G for perception, R_J for memory interaction). Gaussian kernels are chosen for their analytical tractability, smoothness, and biological plausibility for processes where influence decays with distance (Bell 1991; Codling et al. 2008). The periodization is a critical feature that ensures mathematical compatibility with the domain's periodicity and that the convolution of periodic functions remains periodic (Murray 2002). **A crucial consequence of this construction is that the kernel is normalized to unity over a single period, i.e., $\int_0^L K_p(z; R_K)\, dz = 1$.**

After applying the Fourier transform, the convolution operation becomes a simple product in the frequency domain. The Fourier series coefficients of the periodized Gaussian kernel $K_p(z; R_K)$, known as the Fourier symbols, are given by:

$$\hat{K}_p(k) = \exp\left(-\frac{1}{2} R_K^2 k^2\right), \tag{2.6}$$

where $k = 2\pi n/L$ for integers n. This expression makes the smoothing effect of the convolution transparent: as the spatial frequency $|k|$ increases, the symbol $\hat{K}_p(k)$ decays rapidly to zero. This means that the kernel acts as a low-pass filter, attenuating high-frequency (i.e., sharp) details in the function it is convolved with, which is the mathematical basis for the "blurring" or "smoothing" effect of perception and memory generalization.

Based on the interplay of these components, our analysis will address two fundamental questions. First, from a mathematical perspective, under what conditions does this system support sustainable, recurring migrations? This requires us to rigorously establish the well-posedness of the model and then prove the existence of stable, time-periodic solutions. Second, from an ecological perspective, how do perception and memory interact to shape the emergent migratory patterns? Specifically, we will examine how the relative strengths of perception-driven taxis (governed by parameter α) and memory-guided taxis (governed by parameter γ) enable the population to successfully track, or even anticipate, the movement of the resource peak. To ensure the rigor of our analysis, we will proceed under the following assumptions:

(A1) **Initial Data:** The initial history $u_0(x,s) \in C^{2+\alpha,1+\alpha/2}(\bar{\Omega} \times [-N\tau, 0])$ and initial condition $m_0(x) \in C^{2+\alpha}(\bar{\Omega})$, with $\alpha \in (0,1)$, are non-negative and satisfy periodicity and compatibility conditions.

(A2) **Resource Function:** $r(x,t)$, defined by (2.4) with $x_0(t)$ from (2.3), is defined on $\bar{\Omega} \times [0,\infty)$. As per its definition, $r(x,t)$ is C^∞-smooth, non-negative, L-periodic in x, and T-periodic in t. Furthermore, it is uniformly bounded with all its spatial and temporal derivatives, and it is integrable over the spatial domain $\bar{\Omega}$ for all t.

(A3) **Kernel Functions:** $G_p(z; R_G)$ and $J_p(z; R_J)$, given by (2.5), are C^∞-smooth, L-periodic, with $R_G, R_J > 0$.

(A4) **Parameters:** All parameters $d, \varepsilon, \alpha, \gamma, \rho_i, \tau, \mu_m, N$ are positive constants.

3 Global existence and boundedness of classical solutions

In this section, we analyze the mathematical properties of the cognitive migration model (2.1). Our primary goal is to establish the global existence and regularity of classical solutions, a prerequisite for ensuring the model's biological relevance and predictive capability. The analysis proceeds in three stages: (i) we first prove the local existence of a unique classical solution and derive a corresponding blow-up criterion; (ii) we then obtain key *a priori* estimates valid on finite time intervals; and (iii) we employ these bounds to extend the local solution globally for all time.

3.1 Local existence and blow-up criterion

We begin by establishing the local-in-time well-posedness of the system. The following theorem ensures the existence of a unique classical solution on a short time interval and provides the criterion required to extend this solution to a global one.

Theorem 3.1 (Local existence, uniqueness and blow-up criterion) *Under assumptions (A1)–(A4), system (2.1) admits a unique non-negative classical solution* $(u(x,t), m(x,t))$ *on a maximal time interval* $[0, T_{max})$*, where* $T_{max} \in (0,\infty]$*. The solution has the regularity* $u, m \in C^{2+\alpha,1+\alpha/2}_{\text{loc}}(\bar{\Omega} \times [0, T_{max}))$ *and satisfies the periodic boundary conditions. Furthermore, if the maximal time of existence* $T_{max} < \infty$*, then the solution must blow up in the sense that*

$$\limsup_{t \to T_{max}^-} \left(\|u(\cdot,t)\|_{L^\infty(\Omega)} + \|m(\cdot,t)\|_{L^\infty(\Omega)} \right) = \infty. \tag{3.1}$$

Proof We first establish the non-negativity of any potential classical solution. The proof then proceeds by constructing a local-in-time solution using the method of steps and classical theory for parabolic systems, and finally establishing the blow-up criterion.

The non-negativity of the solution (u, m) on its interval of existence follows from an application of the weak maximum principle. We proceed by contradiction. Assume that the solution component $m(x,t)$ is not always non-negative. Since $m(x,0) =$

$m_0(x) \geq 0$ by Assumption (A1) and $m(x,t)$ is continuous, there must be a first time $t_0 > 0$ at which the minimum of m over the spatial domain touches zero before possibly becoming negative. Let us define this first time as

$$t_0 = \inf\{t \in (0, T_{\max}) \mid \min_{x\in\bar{\Omega}} m(x,t) < 0\}.$$

By the continuity of $m(x,t)$, we have $t_0 > 0$ and $\min_{x\in\bar{\Omega}} m(x,t_0) = 0$. Furthermore, there exists a point $x_0 \in \bar{\Omega}$ such that $m(x_0,t_0) = 0$. The point (x_0,t_0) is a minimum point for the function $m(x,t)$ on the domain $\bar{\Omega} \times [0,t_0]$. Therefore, at this point, the derivatives must satisfy:

$$\partial_t m(x_0,t_0) \leq 0 \quad \text{and} \quad \partial_{xx} m(x_0,t_0) \geq 0.$$

The condition on the second spatial derivative holds because, for the fixed time t_0, x_0 is a point of spatial minimum, and the periodic boundary conditions mean the domain is topologically a circle without boundaries where standard conditions for a minimum apply.

Now, we evaluate the m-equation at the point (x_0,t_0):

$$\partial_t m - \varepsilon \partial_{xx} m + \mu_m m = S_m(x,t),$$

where the source term $S_m(x,t)$ is defined as

$$S_m(x_0,t_0) = \frac{1}{N}\sum_{i=1}^{N} \rho_i u(x_0, t_0 - i\tau) h(x_0, t_0 - i\tau).$$

Evaluating the left-hand side of the m-equation at (x_0,t_0), we have:

$$\underbrace{\partial_t m(x_0,t_0)}_{\leq 0} - \underbrace{\varepsilon}_{>0}\underbrace{\partial_{xx} m(x_0,t_0)}_{\geq 0} + \underbrace{\mu_m m(x_0,t_0)}_{=0} \leq 0.$$

Since $t_0 - i\tau < t_0$, $u(x_0, t_0 - i\tau)$ is non-negative by the definition of t_0 as the first time the minimum reaches zero. As h is also non-negative, we have $S_m(x_0,t_0) \geq 0$. This leads to the contradiction $(\leq 0) = (\geq 0)$, which can only hold if both sides are zero. If $S_m(x_0,t_0) > 0$, the contradiction is strict. If $S_m(x_0,t_0) = 0$, a stronger version of the maximum principle (e.g., Hopf's Lemma, adapted for parabolic equations) would be needed to show that this also leads to a contradiction unless m was identically zero, which is not the case if $m_0 \not\equiv 0$. Therefore, our initial assumption that m could become negative must be false. A similar argument holds for the u-equation. Thus, the solution components (u,m) remain non-negative.

We now proceed with the core of the proof: establishing the existence and uniqueness of such a classical solution on a short time interval using the method of steps.

1. Existence of the solution on an initial interval $[0,T_1]$: We first establish the existence of a unique solution on a short time interval. Let $\tau > 0$ be the fundamental

delay period. Our strategy is to first solve for $m(x,t)$ on the interval $[0,\tau]$ and then use this result to solve for $u(x,t)$.

For any $t \in [0,\tau]$, the source term $S_m(x,t)$ in the m-equation is entirely determined by the known non-negative initial history $u_0(x,s)$ for $s \le 0$. Given the smoothness assumed in (A1) and (A2), $S_m(x,t)$ is a known, smooth, and non-negative function in $C^{\alpha,\alpha/2}(\bar{\Omega}\times[0,\tau])$. The m-equation,

$$m_t - \varepsilon m_{xx} + \mu_m m = S_m(x,t),$$

thus becomes a linear parabolic equation with a smooth initial condition $m_0(x) \in C^{2+\alpha}(\Omega)$ and a known smooth source term S_m. Standard theory for linear parabolic equations (e.g., (Ladyzhenskaya and Solonnikov, 1968, Chapter IV)) guarantees the existence of a unique classical solution $m(x,t) \in C^{2+\alpha,1+\alpha/2}(\bar{\Omega}\times[0,\tau])$ on the full interval $[0,\tau]$.

With $m(x,t)$ now known and of class $C^{2+\alpha,1+\alpha/2}$ on $[0,\tau]$, we can analyze the u-equation. This is a quasilinear equation whose lower-order coefficients depend on h and $M_J = m * J_p$. Since h, m, and the kernel J_p are smooth, the coefficients of the u-equation are well-defined and belong to the Hölder space $C^{\alpha,\alpha/2}(\bar{\Omega}\times[0,\tau])$. For a quasilinear parabolic equation with a smooth initial condition $u_0(x,0) \in C^{2+\alpha}(\Omega)$ and coefficients in $C^{\alpha,\alpha/2}$, standard theory (e.g., (Ladyzhenskaya and Solonnikov, 1968, Chapter V)) ensures the existence of a unique classical solution $u(x,t) \in C^{2+\alpha,1+\alpha/2}$ on some (possibly smaller) time interval $[0,\delta_1]$, where $\delta_1 > 0$. By taking $T_1 = \min(\tau,\delta_1)$, we have established the existence of a unique classical solution (u,m) on the interval $[0,T_1]$.

2. Continuation to a maximal interval of existence $[0,T_{\max})$: The procedure above can be iterated. Suppose the solution has been constructed on $[0,T_k]$ for some $T_k \ge T_1$. On the next interval $[T_k, T_k+\tau]$, the source term $S_m(x,t)$ is again determined by the now-known solution u on $[0,T_k]$. We can thus first solve for m on $[T_k, T_k+\tau]$ and then solve for u on a subsequent short time interval. This method of steps allows the solution to be extended to a maximal time interval $[0,T_{\max})$, where $T_{\max} = \sup\{T_k\}$.

3. Blow-up criterion: The blow-up criterion (3.1) is established by a standard continuation argument based on a proof by contradiction. We assume that the maximal time of existence $T_{\max}$ is finite, and yet the solution remains uniformly bounded in L^∞, i.e., there exists a constant $K < \infty$ such that

$$\sup_{t\in[0,T_{\max})} \left(\|u(\cdot,t)\|_{L^\infty(\Omega)} + \|m(\cdot,t)\|_{L^\infty(\Omega)}\right) \le K. \tag{3.2}$$

We will show that this assumption implies uniform bounds on higher-order Hölder norms of the solution up to any time $T_S < T_{\max}$, which ultimately contradicts the maximality of $T_{\max}$. This is achieved through a bootstrapping argument that leverages parabolic regularity theory (see, e.g., Ladyzhenskaya and Solonnikov (1968); Friedman (1964)).

First, we establish the Hölder regularity of the source term S_m in the m-equation. The functions u_0 and h are known to be of class $C^{2+\alpha,1+\alpha/2}$ with bounded norms. For the evolving solution $u(x,t)$ with $t > 0$, while only assumed to be in L^∞ by (3.2),

the smoothing property of parabolic equations with smooth initial data ($u_0(x,0) \in C^{2+\alpha}(\Omega)$) and spatially regular coefficients ensures that u attains $C^{\alpha,\alpha/2}$ regularity for $t > 0$. Its norm in this space, $\|u\|_{C^{\alpha,\alpha/2}(\bar{\Omega}\times(0,T_S])}$, can be bounded by a constant $C_u^{(\alpha)}$ that depends on K and $\|u_0\|_{C^{2+\alpha}(\Omega)}$. By applying the standard product rule for Hölder spaces to each term $u(x,t-i\tau)h(x,t-i\tau)$ in S_m, and combining the estimates for the initial history part ($t - i\tau \leq 0$) and the evolved part ($t - i\tau > 0$), we conclude that $S_m \in C^{\alpha,\alpha/2}(\bar{\Omega}\times[0,T_S])$ for any $T_S < T_{\max}$, with its norm uniformly bounded by a constant $C_S^{(\alpha)}$ depending on K and initial data norms.

With the source term S_m now known to be in $C^{\alpha,\alpha/2}$, we can apply standard Schauder estimates (e.g., (Ladyzhenskaya and Solonnikov, 1968, Chapter IV, Theorem 10.1)) to the linear m-equation,

$$m_t - \varepsilon m_{xx} + \mu_m m = S_m.$$

Given the initial condition $m_0 \in C^{2+\alpha}(\Omega)$ and the $C^{\alpha,\alpha/2}$ regularity of S_m, this theory yields that the solution $m \in C^{2+\alpha,1+\alpha/2}(\bar{\Omega}\times[0,T_S])$ for any $T_S < T_{\max}$. The norm of m in this space, $\|m\|_{C^{2+\alpha,1+\alpha/2}}$, is uniformly bounded by a constant M_m that depends on $\|m_0\|_{C^{2+\alpha}(\Omega)}$ and $C_S^{(\alpha)}$, and thus ultimately on K and initial data.

Now possessing high regularity for m, we revisit the u-equation,

$$u_t - du_{xx} + A_1 u_x + A_0 u = 0.$$

The coefficients $A_1 = \alpha\partial_x h + \gamma\partial_x M_J$ and $A_0 = \alpha\partial_{xx} h + \gamma\partial_{xx} M_J$ involve the term $M_J = m * J_p$. Since $m \in C^{2+\alpha,1+\alpha/2}$ and the kernel $J_p \in C^\infty$, the convolution M_J and its spatial derivatives will also possess high Hölder regularity. Consequently, the coefficients A_1 and A_0 belong to $C^{\alpha,\alpha/2}(\bar{\Omega}\times[0,T_S])$ with uniformly bounded norms.

Finally, we apply Schauder estimates to the u-equation, which is now established as a linear parabolic equation with $C^{\alpha,\alpha/2}$ coefficients. Given the initial condition $u_0(x,0) \in C^{2+\alpha}(\Omega)$, the theory guarantees that the solution $u \in C^{2+\alpha,1+\alpha/2}(\bar{\Omega}\times[0,T_S])$ for any $T_S < T_{\max}$, with a uniformly bounded norm M_u.

This completes the bootstrapping argument: the assumption of a uniform L^∞ bound for (u,m) implies a uniform $C^{2+\alpha,1+\alpha/2}$ bound on any compact time interval $[0,T_S] \subset [0,T_{\max})$. This high regularity ensures that as $t \to T_{\max}^-$, the solution (u,m) converges in the $C^2(\bar{\Omega})$ norm to a limit function (u^*,m^*). This smooth limit function serves as a valid initial condition at $t = T_{\max}$, allowing the local existence result to be applied again to extend the solution beyond $T_{\max}$. This contradicts the maximality of $T_{\max}$. Therefore, the initial assumption (3.2) must be false, which establishes the blow-up criterion (3.1).

Having established the local existence and uniqueness of a non-negative classical solution and the blow-up criterion, the proof of Theorem 3.1 is complete. □

3.2 *A priori* estimates

Theorem 3.1 indicates that to prove global existence ($T_{\max} = \infty$), we must prevent the L^∞-norm of the solution from becoming unbounded in finite time. This requires

establishing *a priori* bounds that are independent of the solution's existence time itself. We begin with some fundamental bounds that are straightforward to obtain.

Lemma 3.2 (Uniform Bounds for L^1-norms and Auxiliary Functions) *Let (u, m) be a solution to system (2.1) on $[0, T_{max})$ under assumptions (A1)–(A4). Then there exists a positive constant M, independent of T_{max}, such that the total mass of the system is uniformly bounded for all $t \in [0, T_{max})$:*

$$\|u(\cdot, t)\|_{L^1(\Omega)} + \|m(\cdot, t)\|_{L^1(\Omega)} \leq M. \tag{3.3}$$

Furthermore, the perceived resource h and its first two spatial derivatives are also uniformly bounded, i.e., there exists a constant $C_h > 0$ such that

$$\|h(\cdot, t)\|_{C^2(\bar{\Omega})} \leq C_h \tag{3.4}$$

for all $t \in [0, T_{max})$.

Proof (i) First, we establish bounds for the individual L^1-norms. Integrating the u-equation over Ω and applying the fundamental theorem of calculus yields

$$\begin{aligned} \frac{d}{dt}\int_\Omega u(x,t)\,dx &= \int_\Omega \left(du_{xx} - \alpha\partial_x(uh_x) - \gamma\partial_x(u\partial_x M_J)\right)\,dx \\ &= \left[du_x(x,t) - \alpha u(x,t)h_x(x,t) - \gamma u(x,t)\partial_x M_J(x,t)\right]\Big|_0^L. \end{aligned} \tag{3.5}$$

The periodic boundary conditions state that $u(0, t) = u(L, t)$ and $u_x(0, t) = u_x(L, t)$. Furthermore, as the convolution of periodic functions (r and G_p), h is also L-periodic in space, and thus its derivative h_x is periodic. Similarly, as the convolution of periodic functions (m and J_p), M_J and its derivative $\partial_x M_J$ are also periodic. Consequently, all terms evaluated at $x = L$ are equal to their counterparts at $x = 0$, causing the boundary terms to vanish. This leads to

$$\frac{d}{dt}\int_\Omega u(x,t)\,dx = 0, \tag{3.6}$$

which implies the conservation of the total population, $\|u(\cdot, t)\|_{L^1(\Omega)} = \|u_0(\cdot, 0)\|_{L^1(\Omega)} := M_u$. Next, we integrate the m-equation over Ω to obtain

$$\frac{d}{dt}\|m(\cdot, t)\|_{L^1(\Omega)} = \int_\Omega S_m(x,t)\,dx - \mu_m\|m(\cdot, t)\|_{L^1(\Omega)}.$$

The integral of the source term is bounded by

$$\int_\Omega S_m(x,t)\,dx \leq \frac{1}{N}\sum_{i=1}^{N}\rho_i\|u(\cdot, t - i\tau)\|_{L^1}\|h(\cdot, t - i\tau)\|_{L^\infty}.$$

The L^1-norm of u is uniformly bounded for all its time arguments. For $s \geq 0$, $\|u(\cdot, s)\|_{L^1} = M_u$ due to conservation. For $s < 0$, $\|u(\cdot, s)\|_{L^1} = \|u_0(\cdot, s)\|_{L^1}$, which

is uniformly bounded on the compact interval $[-N\tau, 0]$ by a constant M_{u0} as a consequence of Assumption (A1). Let $\tilde{M}_u = \max(M_u, M_{u0})$. Furthermore, $\|h\|_{L^\infty}$ is bounded by $\|r\|_{L^\infty} := A_r$ (by Assumption A2). Thus, we have

$$\int_\Omega S_m \, dx \leq \left(\frac{1}{N} \sum_{i=1}^{N} \rho_i \right) \tilde{M}_u A_r := \bar{S}_1. \tag{3.7}$$

The resulting differential inequality,

$$\frac{d}{dt} \|m\|_{L^1} \leq \bar{S}_1 - \mu_m \|m\|_{L^1},$$

implies by Gronwall's inequality that $\|m(\cdot, t)\|_{L^1(\Omega)}$ is uniformly bounded by a constant M_m. Combining the uniform bounds for $\|u\|_{L^1}$ and $\|m\|_{L^1}$ yields the bound M for their sum.

(ii) The uniform bound for h and its derivatives follows directly from the properties of convolution. Since $r \in C^\infty(\mathbb{R} \times \mathbb{R})$ and $G_p \in C^\infty(\mathbb{R})$ are uniformly bounded with all their derivatives (Assumptions A2, A3), their convolution $h(x, t)$ is also uniformly bounded in $C^k(\bar{\Omega})$ for any $k \geq 0$. In particular, there exists a constant C_h such that $\|h(\cdot, t)\|_{C^2(\bar{\Omega})} \leq C_h$ for all t. □

The main challenge is to obtain a bound for the L^∞-norm. While the previous lemma provides essential groundwork, the coupling in the system requires a more intricate argument. The following theorem establishes that the solution remains bounded on any finite time interval.

Theorem 3.3 (*A priori* bound for the L^∞-norm) *Let (u, m) be a classical solution to system (2.1) under assumptions (A1)–(A4). Then for any finite time $\mathcal{T} > 0$, there exists a positive constant $C(\mathcal{T})$, depending on $\mathcal{T}$, as well as on initial data and system parameters, such that:*

$$\sup_{t \in [0, \mathcal{T}]} \left(\|u(\cdot, t)\|_{L^\infty(\Omega)} + \|m(\cdot, t)\|_{L^\infty(\Omega)} \right) \leq C(\mathcal{T}).$$

Proof The proof establishes the existence of a bound $C(\mathcal{T})$ for any given finite time horizon $\mathcal{T} > 0$. This is achieved by constructing the bound through an inductive argument over successive time intervals of length τ. The core of the argument is to show that while the bound may grow with each step, it remains finite for any finite number of steps. Let $C_0 = \max(\|u_0\|_{L^\infty(\Omega \times [-N\tau, 0])}, \|m_0\|_{L^\infty(\Omega)})$. We will construct a sequence of bounds $\{C_k\}_{k \geq 1}$ for the solution on the intervals $[0, k\tau]$.

Base Case: Bound on $[0, \tau]$: For $t \in [0, \tau]$, the source term

$$S_m(x, t) = \sum_{i=1}^{N} \rho_i u(x, t - i\tau) h(x, t - i\tau)$$

in the m-equation depends only on the initial history u_0, which is bounded by C_0. Thus,

$$\|S_m\|_{L^\infty(\Omega\times[0,\tau])} \le \bar{S}_\infty(C_0) := (\frac{1}{N}\sum \rho_i) C_0 C_h,$$

where C_h is the bound for $\|h\|_{C^2}$ from Lemma 3.2. By the maximum principle for the m-equation,

$$\|m(\cdot,t)\|_{L^\infty} \le \max\left\{C_0, \frac{\bar{S}_\infty(C_0)}{\mu_m}\right\} := C_m^{(1)} \quad \text{for } t \in [0,\tau].$$

With this bound for m, we analyze the u-equation, which is a linear parabolic equation for u:

$$\frac{\partial u}{\partial t} - d\frac{\partial^2 u}{\partial x^2} + A_1(x,t)\frac{\partial u}{\partial x} + A_0(x,t)u = 0.$$

The zero-order coefficient, given by

$$A_0(x,t) = \alpha \frac{\partial^2 h}{\partial x^2}(x,t) + \gamma \frac{\partial^2 M_J}{\partial x^2}(x,t),$$

is bounded on $[0,\tau]$. Specifically, using Lemma 3.2 and Young's inequality:

$$\begin{aligned}\|A_0(t)\|_{L^\infty} &\le \alpha\|\partial_{xx}h\|_{L^\infty} + \gamma\|m(\cdot,t) * J_p''\|_{L^\infty}\\ &\le \alpha C_h + \gamma\|m(\cdot,t)\|_{L^\infty}\|J_p''\|_{L^1}\\ &\le \alpha C_h + \gamma C_m^{(1)}\|J_p''\|_{L^1}.\end{aligned}$$

Let us denote this upper bound by $B_0^{(1)}$. We can now apply the maximum principle for linear parabolic equations to the u-equation. A standard result stemming from this principle (see, e.g., (Friedman, 1964, Chapter 3, Theorem 7)) provides an estimate for the solution's growth. The principle states that the solution u is controlled by its initial and boundary data, with potential growth driven only by the positive part of the zero-order coefficient, denoted as $A_0^+(x,t) = \max(A_0(x,t),0)$. This leads to the following estimate for $t \in [0,\tau]$:

$$\begin{aligned}\|u(\cdot,t)\|_{L^\infty(\Omega)} &\le \|u_0(\cdot,0)\|_{L^\infty(\Omega)} \exp\left(\int_0^t \|A_0^+(s)\|_{L^\infty(\Omega)} ds\right)\\ &\le C_0 \exp\left(\int_0^t B_0^{(1)} ds\right)\\ &= C_0 e^{B_0^{(1)} t} \le C_0 e^{B_0^{(1)}\tau} := C_u^{(1)}. \end{aligned} \tag{3.8}$$

In the second inequality, we used the fact that $A_0^+(s) \le |A_0(s)| \le \|A_0(s)\|_{L^\infty} \le B_0^{(1)}$. Thus, for any $t \in [0,\tau]$, the sum of the norms is bounded by

$$\|u(\cdot,t)\|_{L^\infty(\Omega)} + \|m(\cdot,t)\|_{L^\infty(\Omega)} \le C_u^{(1)} + C_m^{(1)}.$$

Let us define the bound for the first step as $C_1 := C_u^{(1)} + C_m^{(1)}$. This bound is a finite constant that is determined *a priori* by the initial data (C_0), system parameters, and the step length τ.

Inductive Step: The procedure described above for the interval $[0, \tau]$ can be iterated for subsequent intervals $[\tau, 2\tau]$, $[2\tau, 3\tau]$, and so on. To formalize this, we proceed by induction.

Assume that for some integer $k \geq 1$, a finite bound C_k has been established for the solution on $[0, k\tau]$. We now construct a bound on the next interval $[k\tau, (k+1)\tau]$. For $t \in [k\tau, (k+1)\tau]$, the source term S_m depends on $u(s)$ for $s \leq k\tau$. By the induction hypothesis, $\|u(s)\|_\infty \leq C_k$. Consequently, $\|S_m\|_{L^\infty} \leq \bar{S}_\infty(C_k)$. Applying the maximum principle, we find a bound for m on $[k\tau, (k+1)\tau]$:

$$\|m(\cdot, t)\|_{L^\infty} \leq \max\left\{\|m(\cdot, k\tau)\|_\infty, \frac{\bar{S}_\infty(C_k)}{\mu_m}\right\} \leq \max\left\{C_k, \frac{\bar{S}_\infty(C_k)}{\mu_m}\right\} := C_m^{(k+1)}.$$

With this bound on m, the coefficient A_0 is bounded on $[k\tau, (k+1)\tau]$ by a constant $B_0^{(k+1)}$. The maximum principle for u then gives:

$$\|u(\cdot, t)\|_{L^\infty} \leq \|u(\cdot, k\tau)\|_\infty e^{B_0^{(k+1)}(t-k\tau)} \leq C_k e^{B_0^{(k+1)}\tau} := C_u^{(k+1)}.$$

We define the bound on $[0, (k+1)\tau]$ as

$$C_{k+1} = \max\left\{C_k, C_m^{(k+1)} + C_u^{(k+1)}\right\}.$$

Since C_k is finite by assumption, and the operations used to define $C_m^{(k+1)}$ and $C_u^{(k+1)}$ (max, addition, multiplication, exponentiation) all map finite numbers to finite numbers, C_{k+1} is also a finite constant.

The inductive procedure above constructs a sequence of finite constants $C_1, C_2, \ldots, C_k, \ldots$ *a priori*, using only the initial data and system parameters. The induction shows that if the solution exists on an interval $[0, k\tau]$, its L^∞-norm is bounded by C_k. Crucially, this bound C_k depends on the number of steps, k, and the step length τ, reflecting the potential for growth over time.

Now, let any finite time $\mathcal{T} > 0$ be given. We can choose an integer $k_T = \lceil \mathcal{T}/\tau \rceil$. Our constructive process yields a finite constant C_{k_T}. The inductive proof guarantees that any classical solution existing on the interval $[0, k_T\tau]$ (which contains $[0, \mathcal{T}]$) is bounded by C_{k_T}. Therefore, we can define the desired bound $C(\mathcal{T}) := C_{k_T}$. This constant depends on $\mathcal{T}$ (via the number of steps k_T) but is finite for any finite $\mathcal{T}$. This establishes that the solution cannot blow up in finite time, as its norm is always controlled by a pre-computable, finite constant on any finite time interval. This completes the proof of the theorem. □

3.3 Global solutions

With the local existence framework and the crucial *a priori* bounds in hand, we are now in a position to prove the main result of this section: the global existence and higher-order regularity of the solution.

Theorem 3.4 (Global Existence and Finite-Time Boundedness) *Under assumptions (A1)–(A4), system (2.1) admits a unique, non-negative, global classical solution* (u, m) *for all time* $t > 0$. *Furthermore, this solution possesses* $C^{2+\alpha,1+\alpha/2}$ *regularity on any finite time interval. That is, for any* $\mathcal{T} \in (0, \infty)$, *there exists a constant* $M(\mathcal{T})$ *such that*

$$\|u\|_{C^{2+\alpha,1+\alpha/2}(\bar{\Omega}\times[0,\mathcal{T}])} + \|m\|_{C^{2+\alpha,1+\alpha/2}(\bar{\Omega}\times[0,\mathcal{T}])} \leq M(\mathcal{T}).$$

Proof The proof consists of two main parts. First, we establish global existence by showing that the solution cannot blow up in finite time, using a continuation argument. Second, we establish the bound on the higher-order Hölder norms.

To begin, Theorem 3.1 guarantees the existence of a unique non-negative classical solution (u, m) on a maximal time interval $[0, T_{\max})$, and provides a blow-up criterion stating that the L^∞-norm must become unbounded if $T_{\max}$ is finite. However, Theorem 3.3 establishes that for any finite time $\mathcal{T} > 0$, any solution existing on $[0, \mathcal{T}]$ must have its L^∞-norm bounded by a constant $C(\mathcal{T})$. Assuming, for the sake of contradiction, that $T_{\max} < \infty$, this would imply that the solution is bounded in L^∞ on the entire interval $[0, T_{\max})$, leading to

$$\limsup_{t\to T_{\max}^-} (\|u(\cdot,t)\|_{L^\infty} + \|m(\cdot,t)\|_{L^\infty}) < \infty.$$

This result directly contradicts the blow-up criterion from Theorem 3.1. Therefore, the assumption that $T_{\max}$ is finite must be false, and we conclude that $T_{\max} = \infty$. This proves the global existence of the solution.

With global existence established, we now demonstrate the bound on the higher-order Hölder norms. This follows from a standard bootstrapping argument, leveraging the now-known L^∞ bound on any finite interval $[0, \mathcal{T}]$ from Theorem 3.3. The logic is identical to the regularity enhancement argument used to justify the blow-up criterion. Specifically, for any given $\mathcal{T} > 0$, the L^∞ bound $C(\mathcal{T})$ ensures that the source term S_m in the m-equation belongs to $C^{\alpha,\alpha/2}(\bar{\Omega} \times [0, \mathcal{T}])$, with a norm depending on $C(\mathcal{T})$. Applying Schauder estimates to the linear m-equation with this regular source term then yields a bound for $\|m\|_{C^{2+\alpha,1+\alpha/2}(\bar{\Omega}\times[0,\mathcal{T}])}$, which we denote by $M_m(\mathcal{T})$. This high regularity of m in turn ensures that the coefficients of the u-equation are of class $C^{\alpha,\alpha/2}(\bar{\Omega} \times [0, \mathcal{T}])$. A final application of Schauder estimates to the now-linear u-equation with these regular coefficients yields a bound for $\|u\|_{C^{2+\alpha,1+\alpha/2}(\bar{\Omega}\times[0,\mathcal{T}])}$, denoted by $M_u(\mathcal{T})$. By setting $M(\mathcal{T}) = M_u(\mathcal{T}) + M_m(\mathcal{T})$, we obtain the desired bound on the $C^{2+\alpha,1+\alpha/2}$-norm of the solution. This completes the proof. □

4 Existence and stability of periodic solutions

Having established the global well-posedness of the initial value problem, we now examine the system's long-term dynamics. Given the time-periodic nature of the external resource function $r(x,t)$, it is natural to investigate the existence of corresponding time-periodic solutions, which represent stable, recurring migratory patterns. This section focuses on proving the existence of such a solution, while the subsequent analysis addresses its uniqueness and global asymptotic stability.

We begin by establishing the existence of at least one time-periodic solution.

Theorem 4.1 (Existence of Time-Periodic Solutions) *Assume that (A1)–(A4) hold, and let $T > 0$ be the period of the external resource function $r(x,t)$ with respect to time. Then, system (2.1) admits at least one non-negative, classical solution $(u^*(x,t), m^*(x,t))$ that is periodic in both time and space. This solution satisfies the time-periodicity condition*

$$u^*(\cdot, t+T) = u^*(\cdot,t), \quad m^*(\cdot,t+T) = m^*(\cdot,t) \ \ \textit{for all } t \geq 0,$$

and the spatial-periodicity condition

$$u^*(x+L,t) = u^*(x,t), \quad m^*(x+L,t) = m^*(x,t) \ \ \textit{for all } x,t.$$

Furthermore, this periodic solution possesses the regularity $u^*, m^* \in C^{2+\alpha,1+\alpha/2}(\bar{\Omega}\times[0,\infty))$.

Proof The proof is based on the Leray-Schauder fixed-point theorem, which requires reformulating the problem in a suitable functional setting and establishing uniform *a priori* bounds for all possible periodic solutions to a family of problems.

1. Fixed-point formulation: We seek a classical solution that is periodic in both space and time. As stated in the theorem, let $T > 0$ be the period of the external forcing term $r(x,t)$. We define the Banach space X for our problem as the space of Hölder continuous functions that satisfy the required periodicity:

$$X := \left\{ \phi \in C^{1+\beta,(1+\beta)/2}(\bar{\Omega}\times\mathbb{R}) \mid \phi \text{ is } L\text{-periodic in } x \text{ and } T\text{-periodic in } t \right\}, \tag{4.1}$$

for some fixed $\beta \in (0,\alpha)$. The norm on the product space $X \times X$ is given by $\|(\phi_1,\phi_2)\|_{X\times X} = \|\phi_1\|_X + \|\phi_2\|_X$. We seek a fixed point for an operator within the cone of non-negative functions in $X \times X$.

To apply the Leray-Schauder theorem, we define a family of operators $\mathcal{F}_\lambda : X \times X \to X \times X$ for a homotopy parameter $\lambda \in [0,1]$. The action of an operator $\mathcal{F}_\lambda$ on a given pair $(\tilde{u},\tilde{m}) \in X \times X$ is defined through the unique T-periodic solution (u,m) of the auxiliary linear parabolic system:

$$\begin{cases} \partial_t u - d\partial_{xx}u + u = \lambda\left[-\alpha\partial_x(\tilde{u}\partial_x h) - \gamma\partial_x(\tilde{u}\partial_x(\tilde{m} * J_p))\right] + \tilde{u}, \\ \partial_t m - \varepsilon\partial_{xx}m + \mu_m m = \lambda S_m(\tilde{u},h), \end{cases} \tag{4.2}$$

where $S_m(\tilde{u}, h) = \frac{1}{N}\sum_{i=1}^{N} \rho_i \tilde{u}(x, t - i\tau)h(x, t - i\tau)$. That is, we set $(u, m) := \mathcal{F}_\lambda(\tilde{u}, \tilde{m})$. The operator $\mathcal{L}_u := \partial_t - d\partial_{xx} + 1$ is invertible on the space of T-periodic functions, ensuring a unique periodic solution u for any given right-hand side. Similarly, since $\mu_m > 0$, the operator $\mathcal{L}_m := \partial_t - \varepsilon\partial_{xx} + \mu_m$ is also invertible on this space. Thus, for any right-hand side in $C^{\beta,\beta/2}$, system (4.2) admits a unique T-periodic solution (u, m) in $C^{2+\beta,(2+\beta)/2}$.

We must verify that the operator $\mathcal{F}_\lambda$ is completely continuous (i.e., compact and continuous) on the space $X \times X$.

To establish compactness, we consider a bounded set of inputs $(\tilde{u}, \tilde{m})$ in $X \times X$. The right-hand side of the auxiliary system (4.2) is then bounded in the space $C^{\beta,\beta/2}$. By applying standard Schauder estimates for linear parabolic equations with periodic conditions, we find that the corresponding set of solutions (u, m) is bounded in the higher-order space $C^{2+\beta,(2+\beta)/2}$. The Arzelà-Ascoli theorem implies that the embedding from $C^{2+\beta,(2+\beta)/2}$ into our working space $X = C^{1+\beta,(1+\beta)/2}$ is compact. Therefore, the operator $\mathcal{F}_\lambda$ maps bounded sets into precompact sets, establishing its compactness for each $\lambda \in [0, 1]$.

Furthermore, the operator $\mathcal{F}_\lambda$ is continuous with respect to both the input functions $(\tilde{u}, \tilde{m})$ and the parameter λ. This follows from the classical result on the continuous dependence of solutions to linear parabolic equations on their data and coefficients.

A T-periodic solution to our original system (2.1) is a fixed point of the operator at $\lambda = 1$, i.e., a solution to the equation $(u, m) = \mathcal{F}_1(u, m)$.

2. *A priori* bounds for periodic solutions: The crucial step in applying the Leray-Schauder theorem is to establish a uniform *a priori* bound for all possible T-periodic solutions to the fixed-point problem $(u, m) = \mathcal{F}_\lambda(u, m)$, for any $\lambda \in [0, 1]$. Such a solution (u, m) satisfies the homotopy system:

$$\begin{cases} \frac{\partial u}{\partial t} = du_{xx} - \lambda\left(\alpha\partial_x(uh_x) + \gamma\partial_x(u\partial_x(m * J_p))\right), \\ \frac{\partial m}{\partial t} = \varepsilon m_{xx} - \mu_m m + \lambda S_m(u, h), \end{cases} \tag{4.3}$$

where $S_m(u, h) = \frac{1}{N}\sum_{i=1}^{N} \rho_i u(x, t - i\tau)h(x, t - i\tau)$. Establishing a uniform bound for any solution to (4.3), independent of λ, ensures that no fixed points lie on the boundary of a sufficiently large open set in our Banach space, a key requirement for the topological degree argument.

Our proof strategy is a direct adaptation of the inductive argument used for the initial value problem in Theorem 3.3. For a T-periodic solution, its L^∞-norm over all time is achieved on the compact interval $[0, T]$, so we can apply the iterative bounding procedure on this representative interval.

The key observation is that the homotopy parameter $\lambda \in [0, 1]$ only appears as a prefactor to the terms that can drive solution growth. Since $\lambda \leq 1$, the magnitude of these terms is always less than or equal to their magnitude in the original system (where $\lambda = 1$). Consequently, any upper bound derived for the case $\lambda = 1$ will also serve as a valid upper bound for the homotopy system for any $\lambda \in [0, 1]$.

More precisely, let (u, m) be any T-periodic solution to (4.3). Let C_0 be the upper bound for the L^∞-norm of the initial function as in Theorem 3.3. In the base case on

$[0, \tau]$, the source term for the m-equation is λS_m, so its bound

$$\|\lambda S_m\|_{L^\infty} \leq \lambda \bar{S}_\infty(C_0) \leq \bar{S}_\infty(C_0).$$

The subsequent bound $C_m^{(1)}$ is therefore controlled by a constant constructed in the same way as in the proof of Theorem 3.3. Similarly, in the u-equation, the advection terms are multiplied by λ. Since $\lambda \leq 1$, the bound $B_0^{(1)}$ for the coefficient A_0 will also be less than or equal to the one computed for $\lambda = 1$. Thus, the resulting bound $C_u^{(1)}$ is also controlled. This means that the *a priori* constants $C_m^{(1)}$ and $C_u^{(1)}$, which were constructed in the proof of Theorem 3.3, are also valid upper bounds for the solution of the homotopy system on $[0, \tau]$.

This logic extends to every step of the induction. At each step k, the presence of $\lambda \leq 1$ only serves to decrease the magnitude of the terms driving growth. Therefore, the sequence of *a priori* bounds $\{C_k\}$ constructed in the proof of Theorem 3.3 serves as a valid upper bound for any possible T-periodic solution, independent of λ. Since the number of steps required to cover the period $[0, T]$ is finite ($k_T = \lceil T/\tau \rceil$), the resulting bound $C(T) = C_{k_T}$ is a finite constant that depends on the period T and the fundamental system parameters (as the initial data scale for periodic solutions can ultimately be controlled by the L^1-norm M_u), and is independent of the specific solution and the parameter λ. We can therefore define a uniform constant $R := C(T)$ that bounds any possible T-periodic solution of (4.3).

Finally, a standard bootstrapping argument using Schauder estimates upgrades this uniform L^∞ bound to a uniform bound in the X-norm, $\|(u, m)\|_X < R_X$, for some constant R_X also independent of λ.

3. Application of the Leray-Schauder theorem: With the uniform *a priori* bound established in the previous step, we are now in a position to apply the Leray-Schauder fixed-point theorem. Let R_X be the uniform bound for the norm in the space $X \times X$, which was shown to be independent of λ. We define a large, open, bounded set $\mathcal{B} \subset X \times X$ by

$$\mathcal{B} = \{(u, m) \in X \times X \mid \|(u, m)\|_{X\times X} < R_X + 1\}.$$

Our *a priori* estimate from Step 2 guarantees that there are no solutions to the fixed-point problem $(u, m) = \mathcal{F}_\lambda(u, m)$ on the boundary $\partial\mathcal{B}$ for any $\lambda \in [0, 1]$. This is the key condition for the homotopy invariance property of the Leray-Schauder degree, which states that

$$\deg(I - \mathcal{F}_1, \mathcal{B}, 0) = \deg(I - \mathcal{F}_0, \mathcal{B}, 0).$$

The problem is thus reduced to computing the degree for the simpler case $\lambda = 0$. For $\lambda = 0$, the fixed-point equation $(u, m) = \mathcal{F}_0(u, m)$ is equivalent to the linear system

$$u_t - du_{xx} + u = u, \quad m_t - \varepsilon m_{xx} + (\mu_m + 1)m = m.$$

This simplifies to $u_t - du_{xx} = 0$ and $m_t - \varepsilon m_{xx} + \mu_m m = 0$. The only T-periodic solution to the second equation is $m \equiv 0$. For the first equation, any constant $u \equiv c$ is a solution. If we consider the problem in a space of fixed mass $M_u > 0$, the only solution

is $(M_u/L, 0)$. A detailed analysis of the linearization of $\mathcal{F}_0$ around this solution shows that its index is non-zero (specifically 1). Therefore, $\deg(I - \mathcal{F}_0, \mathcal{B}, 0) \neq 0$.

By homotopy invariance, it follows that $\deg(I - \mathcal{F}_1, \mathcal{B}, 0) \neq 0$. A fundamental property of the topological degree is that a non-zero degree implies the existence of at least one solution to the equation $(u, m) = \mathcal{F}_1(u, m)$ inside the ball $\mathcal{B}$.

This establishes the existence of at least one non-trivial, T-periodic solution (u^*, m^*). The non-negativity of this solution is guaranteed by our *a priori* analysis using the maximum principle. The fixed-point theorem ensures the solution belongs to our working space $X = C^{1+\beta,(1+\beta)/2}$. The asserted higher-order regularity, $u^*, m^* \in C^{2+\alpha,1+\alpha/2}(\bar{\Omega} \times \mathbb{R})$, follows from a standard bootstrapping argument using Schauder estimates, since the solution is now known to be bounded. This completes the proof sketch. □

Remark 4.2 **Distinction in Regularity for Global vs. Periodic Solutions.** It is important to clarify the distinction between the regularity statements in Theorem (3.4) and Theorem (4.1). Theorem (3.4) establishes global existence for all $t > 0$, but the $C^{2+\alpha,1+\alpha/2}$ regularity is claimed on any finite time interval $[0, \mathcal{T}]$, with a bound $M(\mathcal{T})$ that generally depends on the observation horizon $\mathcal{T}$. In contrast, for a T-periodic solution (u^*, m^*), its $C^{2+\alpha,1+\alpha/2}$ regularity holds uniformly for all $t \geq 0$. This is because the solution's dynamics are fully determined by its behavior over a single period $[0, T]$, where T is the period of the external forcing. Consequently, the uniform bounds for periodic solutions depend only on this inherent period T (not on an arbitrary observation horizon $\mathcal{T}$), thus reflecting its uniform regularity over an infinite time horizon.

Having established the existence of at least one non-trivial, time-periodic solution, the natural and crucial subsequent questions concern its uniqueness and global asymptotic stability. If a periodic solution is unique and globally asymptotically stable, it implies that the long-term migratory pattern of the population is robust, predetermined by the environmental conditions, and independent of the initial state (provided the total population mass is the same). This means all solutions, regardless of their starting point, will eventually converge to this single, stable migratory pattern. The following theorem addresses these combined properties, showing that uniqueness and global asymptotic stability can indeed be guaranteed under certain conditions on the system parameters.

Theorem 4.3 (Uniqueness and Global Asymptotic Stability of the Time-Periodic Solution) *Assume that (A1)–(A4) hold. Let $C_P = L/(2\pi)$ be the optimal Poincaré constant for the 1D periodic domain Ω, and let M_m be the uniform a priori bound for the L^1-norm of the memory component, as established in Lemma 3.2. Let the constants c_1 and c_2 be defined as:*

$$c_1 := \frac{2}{d\mu_m}(\gamma R_X \|J_p'\|_{L^1})^2, \quad c_2 := \frac{c_1}{N^2\mu_m}\left(\sum_{i=1}^{N} \rho_i \|h\|_\infty\right)^2. \tag{4.4}$$

where R_X is the a priori L^∞-bound for any periodic solution, established in the proof of Theorem 4.1. If the advection strengths α and γ are sufficiently small, satisfying

$$\alpha\left(\frac{\|h_{xx}\|_\infty C_P^2}{2}\right)+\gamma\left(M_m\|J_p'\|_{L^\infty}C_P\right)+\frac{c_2NC_P^2}{2}<\frac{3d}{4}, \tag{4.5}$$

then system (2.1) admits a unique, non-trivial, non-negative, T-periodic solution $(u^*(x,t),m^*(x,t))$ with total mass M_u. Furthermore, this unique periodic solution is globally asymptotically stable. Specifically, for any non-negative initial data $(u_0(x,s),m_0(x))$ satisfying $\int_\Omega u_0(x,0)dx = M_u$, the corresponding solution $(u(x,t),m(x,t))$ converges to the periodic solution $(u^*(x,t),m^*(x,t))$ as $t\to\infty$, in the sense that

$$\lim_{t\to\infty}\|u(\cdot,t)-u^*(\cdot,t)\|_{L^\infty(\Omega)}=0 \quad \textit{and} \quad \lim_{t\to\infty}\|m(\cdot,t)-m^*(\cdot,t)\|_{L^\infty(\Omega)}=0.$$

Proof The proof proceeds by contradiction, using an energy method based on the construction of a suitable Lyapunov-Krasovskii functional. This is a standard technique for analyzing the stability of systems with time delays (see, e.g., Hale (1977); Smith (2011); Jianhong (1996)).

Let $(u^*(x,t),m^*(x,t))$ be any T-periodic solution from Theorem 4.1, and let $(u(x,t),m(x,t))$ be any other global classical solution to system 2.1 originating from initial data (u_0,m_0) that satisfies $\int_\Omega u_0(x,0)dx = M_u$. We define the perturbation functions $\bar{u}=u-u^*$ and $\bar{m}=m-m^*$. Note that $\int_\Omega \bar{u}(x,t)\,dx = 0$ for all $t\geq 0$. The difference functions satisfy the system:

$$\partial_t\bar{u}=d\bar{u}_{xx}-\alpha\partial_x(\bar{u}h_x)-\gamma\partial_x\left(\bar{u}\partial_x(m*J_p)+u^*\partial_x(\bar{m}*J_p)\right) \tag{4.6}$$

$$\partial_t\bar{m}=\varepsilon\bar{m}_{xx}-\mu_m\bar{m}+\frac{1}{N}\sum_{i=1}^{N}\rho_i\bar{u}(x,t-i\tau)h(x,t-i\tau) \tag{4.7}$$

We introduce the Lyapunov-Krasovskii functional

$$\mathcal{E}(t)=\frac{1}{2}\int_\Omega\left(\bar{u}^2(x,t)+c_1\bar{m}^2(x,t)\right)dx+\frac{c_2}{2}\sum_{i=1}^{N}\int_{t-i\tau}^{t}\int_\Omega\bar{u}^2(x,s)\,dxds,$$

where c_1, c_2 are the positive constants defined in (4.4). Differentiating $\mathcal{E}(t)$ with respect to time, we get:

$$\frac{d\mathcal{E}}{dt}=\int_\Omega\bar{u}\partial_t\bar{u}\,dx+c_1\int_\Omega\bar{m}\partial_t\bar{m}\,dx+\frac{c_2}{2}\sum_{i=1}^{N}\left(\|\bar{u}(t)\|_2^2-\|\bar{u}(x,t-i\tau)\|_2^2\right).$$

We now estimate the integrals of the difference equations. Let R_X be the uniform *a priori* C^1-bound for periodic solutions, so that $\|u^*\|_\infty$, $\|m_x^*\|_\infty$, etc., are bounded by R_X.

Multiplying (4.7) by $c_1\bar{m}$ and integrating over Ω gives

$$c_1\int_\Omega \bar{m}\partial_t\bar{m}\,dx = -c_1\varepsilon\|\bar{m}_x\|_2^2 - c_1\mu_m\|\bar{m}\|_2^2 + \frac{c_1}{N}\sum\rho_i\int_\Omega \bar{m}(t)\bar{u}(x,t-i\tau)h(x,t-i\tau)\,dx.$$

Using Young's inequality on the last term for each i:

$$\left|\frac{c_1}{N}\rho_i\int \bar{m}(t)\bar{u}(x,t-i\tau)h(x,t-i\tau)\,dx\right| \le \frac{c_1\rho_i\|h\|_\infty}{N}\left(\frac{\eta}{2}\|\bar{m}(t)\|_2^2 + \frac{1}{2\eta}\|\bar{u}(x,t-i\tau)\|_2^2\right).$$

Summing over i and choosing η such that $\sum\frac{c_1\rho_i\|h\|_\infty}{N}\frac{\eta}{2} = \frac{c_1\mu_m}{2}$, we can absorb half of the decay term. This leaves

$$c_1\int_\Omega \bar{m}\partial_t\bar{m}\,dx \le -c_1\varepsilon\|\bar{m}_x\|_2^2 - \frac{c_1\mu_m}{2}\|\bar{m}\|_2^2 + \frac{c_2}{2}\sum_{i=1}^{N}\|\bar{u}(x,t-i\tau)\|_2^2.$$

Multiplying (4.6) by $\bar{u}$ and integrating by parts yields

$$\int_\Omega \bar{u}\partial_t\bar{u}\,dx = -d\|\bar{u}_x\|_2^2 - \frac{\alpha}{2}\int_\Omega h_{xx}\bar{u}^2\,dx + \gamma\int_\Omega \bar{u}_x\left(\bar{u}(m*J_p') + u^*(\bar{m}*J_p')\right)dx.$$

We bound the last three terms using Hölder, Young, and Poincaré inequalities ($\|\bar{u}\|_2 \le C_P\|\bar{u}_x\|_2$):

$$\begin{aligned}
\left|-\frac{\alpha}{2}\int_\Omega h_{xx}\bar{u}^2dx\right| &\le \frac{\alpha}{2}\|h_{xx}\|_{L^\infty}\|\bar{u}\|_2^2 \le \frac{\alpha\|h_{xx}\|_{L^\infty}C_P^2}{2}\|\bar{u}_x\|_2^2.\\
\left|\gamma\int_\Omega \bar{u}_x\bar{u}(m*J_p')dx\right| &\le \gamma\|m*J_p'\|_{L^\infty}\|\bar{u}_x\|_2\|\bar{u}\|_2 \le \gamma\|m\|_{L^\infty}\|J_p'\|_{L^1}C_P\|\bar{u}_x\|_2^2\\
&\le \gamma M_m\|J_p'\|_{L^1}C_P\|\bar{u}_x\|_2^2.\\
\left|\gamma\int_\Omega \bar{u}_x u^*(\bar{m}*J_p')dx\right| &\le \gamma\|u^*\|_{L^\infty}\|\bar{u}_x\|_2\|\bar{m}*J_p'\|_2 \le \gamma R_X\|\bar{u}_x\|_2\|\bar{m}\|_2\|J_p'\|_{L^1}\\
&\le \frac{d}{4}\|\bar{u}_x\|_2^2 + \frac{(\gamma R_X\|J_p'\|_{L^1})^2}{d}\|\bar{m}\|_2^2 = \frac{d}{4}\|\bar{u}_x\|_2^2 + \frac{c_1\mu_m}{2}\|\bar{m}\|_2^2.
\end{aligned}$$

In the second inequality, we used the fact that the L^1-norm of any solution is uniformly bounded by the constant M_m established in Lemma 3.2. The last equality holds by our choice of c_1 in (4.4).

Summing all estimates for $\frac{d\mathcal{E}}{dt}$, and using Poincaré's inequality on the $\frac{c_2N}{2}\|\bar{u}\|_2^2$ term, we get

$$\frac{d\mathcal{E}}{dt} \le -\left(\frac{3d}{4} - \frac{\alpha\|h_{xx}\|_\infty C_P^2}{2} - \gamma M_m\|J_p'\|_{L^\infty}C_P - \frac{c_2NC_P^2}{2}\right)\|\bar{u}_x\|_2^2 - c_1\varepsilon\|\bar{m}_x\|_2^2.$$

If the condition (4.5) on α and γ holds, the coefficient of $\|\bar{u}_x\|_2^2$ is strictly positive. Let this coefficient be $\lambda_1 > 0$. Then

$$\frac{d\mathcal{E}}{dt} \leq -\lambda_1 \|\bar{u}_x\|_2^2 - c_1 \varepsilon \|\bar{m}_x\|_2^2 \leq 0.$$

Since $\mathcal{E}(t)$ is a non-negative functional, and its time derivative is bounded by negative definite terms involving the L^2-norms of gradients and $\bar{m}$, we can apply Poincaré's inequality (for $\bar{u}$ and $\bar{m}$ terms, as $\int_\Omega \bar{u} dx = 0$) to show that:

$$\frac{d\mathcal{E}}{dt} \leq -\Lambda \mathcal{E}(t)$$

for some positive constant $\Lambda > 0$. By applying Gronwall's inequality, this implies that $\mathcal{E}(t)$ decays exponentially to zero as $t \to \infty$. The decay of $\mathcal{E}(t) \to 0$ then directly implies:

$$\lim_{t\to\infty} \|\bar{u}(\cdot, t)\|_{L^2(\Omega)} = 0 \quad \text{and} \quad \lim_{t\to\infty} \|\bar{m}(\cdot, t)\|_{L^2(\Omega)} = 0.$$

This means the arbitrary solution (u, m) converges to the periodic solution (u^*, m^*) in the L^2-norm.

Finally, the convergence can be upgraded from the L^2-norm to the stronger L^∞-norm. Since the perturbation functions $(\bar{u}, \bar{m})$ solve a linear parabolic system with bounded coefficients, standard interpolation inequalities and regularity estimates for parabolic equations show that their L^∞-norm is controlled by their L^2-norm and the norms of their gradients. As the L^2-norms of both the perturbations and their gradients (as implied by $\mathcal{E}(t) \to 0$ and the decay estimate for $d\mathcal{E}/dt$) tend to zero, it follows that their L^∞-norms also tend to zero. This establishes the global asymptotic stability of the periodic solution.

Now, we deduce the uniqueness of the T-periodic solution from its global asymptotic stability. Assume, for contradiction, that there exist two distinct non-trivial T-periodic solutions, $(u_A^*(x,t), m_A^*(x,t))$ and $(u_B^*(x,t), m_B^*(x,t))$, both with total mass M_u. According to the global asymptotic stability just established (Step 4), any solution originating from an initial condition must converge to $(u_A^*(x,t), m_A^*(x,t))$ as $t \to \infty$. Consider the solution $(u_B^*(x,t), m_B^*(x,t))$. Since it is a solution itself, it must converge to $(u_A^*(x,t), m_A^*(x,t))$ according to the established global asymptotic stability. However, $(u_B^*(x,t), m_B^*(x,t))$ is a T-periodic solution. A T-periodic solution by definition stays on its own closed trajectory and does not "converge" to a different trajectory unless they are identical. Therefore, it must be that $(u_A^*(x,t), m_A^*(x,t)) = (u_B^*(x,t), m_B^*(x,t))$. This contradicts our initial assumption that they were distinct. Thus, the T-periodic solution is unique. This completes the proof of Theorem (4.3). □

Remark 4.4 The argument in the proof of Theorem 4.3 can be interpreted from a dynamical systems viewpoint. Let $\mathcal{P}$ be the period-T Poincaré map that advances any initial data (u_0, m_0) by one full period of the forcing. The unique periodic solution (u^*, m^*) is a fixed point of this map. Our proof, by showing the strict decay of the Lyapunov-Krasovskii functional $\mathcal{E}(t)$ for any solution other than the periodic one, implies that $\mathcal{P}$ is a strict contraction in the norm induced by the functional. That is,

for any initial data $(u_0, m_0) \neq (u^*, m^*)$, the "distance" to the fixed point decreases after one period. By the Banach fixed-point theorem, repeated application of this contraction map ensures that any trajectory will converge to the unique fixed point (u^*, m^*). This brief remark connects our PDE-based proof to the powerful intuition of discrete dynamical systems.

Remark 4.5 The requirement in Theorem 4.3 that the advection strengths α and γ be sufficiently small has a clear biological interpretation. These parameters quantify the intensity of directed movement towards perceived resources and remembered locations, which act as aggregation mechanisms. Our results on uniqueness and global stability suggest that if these aggregation-driving forces are not overly strong relative to the system's inherent dissipative effects—such as random dispersal (d), memory diffusion (ε), and memory decay (μ_m)—the population will inevitably converge to a single, predetermined, and stable migratory pattern, regardless of its initial state. Conversely, strong taxis could potentially lead to multiple stable migratory patterns, where the final outcome depends on historical contingencies.

5 Numerical simulations

In this section, we present a series of numerical simulations of the cognitive migration model (2.1) to illustrate our theoretical results and explore the model's rich cognitive dynamics. Our numerical approach is based on the method of lines. For spatial discretization, we use a pseudo-spectral method with $N_x = 128$ grid points. For time integration, we employ a fourth-order Runge-Kutta (RK4) scheme with a fixed time step of $\Delta t = 0.01$. Convolutions are computed efficiently in Fourier space via the Fast Fourier Transform (FFT); kernels are constructed with periodization to match the domain, and no de-aliasing was found necessary. The time-delay terms are handled by accessing stored historical values via direct indexing. All simulations are conducted on a one-dimensional domain $\Omega = [0, L]$ with periodic boundary conditions, using the baseline parameter values listed in Table 2 unless otherwise specified.

To confirm the convergence of our numerical scheme, a refinement study was conducted for a baseline scenario by halving the time step and doubling the number of grid points. The resulting long-term solution showed no significant qualitative differences from the results presented, confirming that our chosen discretization parameters provide sufficient accuracy. Our investigation is structured into a preliminary analysis of the model's fundamental properties, followed by a detailed deconstruction of its core cognitive mechanisms.

We begin by visually supporting the theoretical results on global asymptotic stability established in Theorems 4.3. To this end, we present a numerical simulation whose primary aim is to illustrate that the long-term behavior of the system is independent of its initial state, consistently converging to a single, stable migratory pattern. As shown in Fig. 1, the simulation is initialized with a non-equilibrium, bimodal population density that is far from the predicted periodic solution. The sequence of snapshots captures the transient dynamics, as the initial distribution progressively diffuses and transforms into a single traveling wave that synchronizes with the resource. The state-space tra-

Table 2 Baseline parameter values for numerical simulations

Parameter	Value	Units	Description
Domain and Environment Parameters			
L	100	space	Spatial domain length
T	365	time	Environmental period (days)
A_r	1.0	resource/space	Resource amplitude
σ_r	8.0	space	Resource spatial width (std. dev.)
Cognitive Parameters			
d	0.2	space^2/time	Population diffusion coefficient
α	0.01	space^2/(time·resource)	Taxis strength towards perceived resource
γ	1.0	space^2/(time·memory)	Taxis strength towards memory
ε	0.2	space^2/time	Memory diffusion coefficient
μ_m	0.1	1/time	Memory decay rate
τ	730	time	Seasonal memory time window
N	5	dimensionless	Number of memory windows
R_G	1.5	space	Perceptual range (std. dev.)
R_J	1.5	space	Memory interaction range (std. dev.)

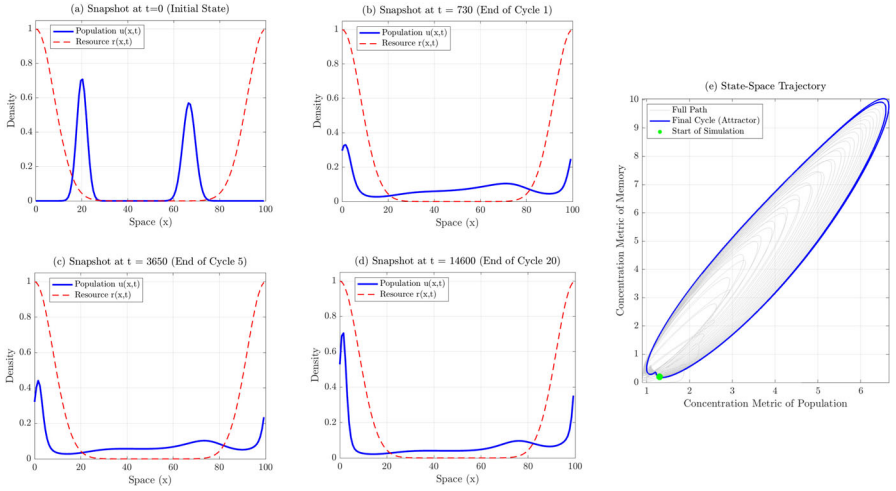

Fig. 1 Illustration of global asymptotic stability and convergence to the periodic attractor. The simulation starts from a non-equilibrium initial population density $u(x, t)$, shown in panel (a), and evolves over time. Panels (b–d) show how the distribution gradually synchronizes with the resource $r(x, t)$, forming a coherent traveling wave. Panel (e) presents the trajectory in state space, where the concentration metrics reveal convergence from an arbitrary initial state (green dot) to the stable limit cycle, confirming the emergence of the unique periodic solution

jectory (Fig. 1e), whose axes represent concentration metrics based on the squared L^2-norms of the population and memory, provides compelling visual confirmation of this convergence. The trajectory initially follows a spiraling path, reflecting the decay of transient dynamics, before settling into a closed loop—a limit cycle attractor—representing the unique, globally asymptotically stable periodic solution predicted by our theoretical analysis.

To justify our subsequent focus on the cognitive parameters, we performed a global sensitivity analysis using the Fourier Amplitude Sensitivity Test (FAST). This method attributes the variance in the model's output to the uncertainty in each input parameter. For this analysis, all parameters were varied by $\pm 50\%$ around their baseline values (Table 2) with a sample size of $N_s = 1025$. This analysis quantitatively validates that cognitive migration is fundamentally shaped by the interplay between perception and memory. As seen in Fig. 2, perception-driven taxis (α) emerges as the dominant contributor to movement efficiency, reflecting the crucial role of responding to the instantaneous resource gradient. At the same time, the memory subsystem governed primarily by the delay parameter τ, which sets the temporal horizon of past experience, and secondarily by the memory-taxis strength γ, exerts a substantial influence on how animals accumulate, retain, and act upon historical foraging information. Together, these findings confirm that it is the combined action of perception-based and memory-based movement mechanisms that underlies the adaptive dynamics of the model, with perception shaping immediate responsiveness and memory shaping long-term anticipatory behavior.

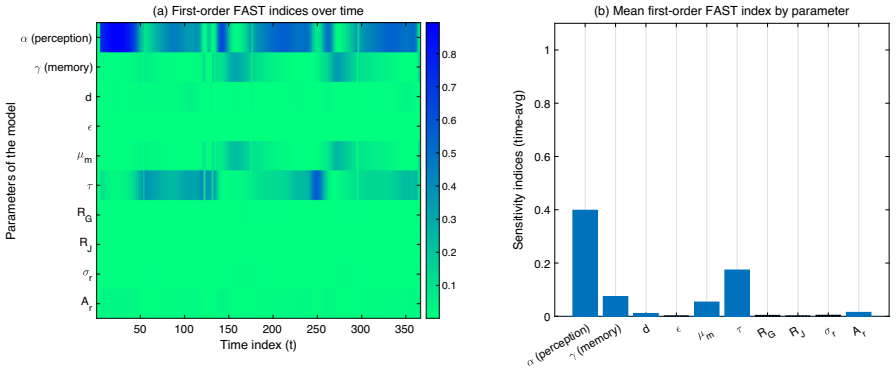

Fig. 2 Global sensitivity analysis of model parameters. (Left) First-order FAST sensitivity indices for each parameter calculated over the course of the simulation. Darker colors (blue) indicate higher influence on the model output. (Right) The time-averaged mean of the first-order sensitivity indices, providing a summary of each parameter's overall importance

Guided by these preliminary analyses, which highlight the paramount importance of taxis strengths, the remainder of this section is dedicated to a detailed deconstruction of the core cognitive mechanisms. We proceed in three subsections, beginning with an in-depth analysis of the interplay between perception (α) and memory (γ), followed by investigations into the roles of memory precision (ε) and memory timescale (τ).

Before analyzing the cognitive strategies, we first establish the environmental context that remains constant across all subsequent experiments. Figure 3 displays the spatio-temporal dynamics of the prescribed resource distribution, $r(x, t)$, and the corresponding perceived landscape, $h(x, t)$, generated using the baseline parameters in Table 2. The resource, $r(x, t)$, is modeled as a traveling Gaussian pulse that completes a unidirectional circuit on the domain $\Omega = [0, L]$ over a period T. Note that we regard $x = 0$ and $x = L$ as representing the same physical location. This is visually evident from the migratory paths shown on the cylinder in Fig. 3 (a) and (b) unfolds the cylinder into a plane, where movement from $x = 0$ to $x = L$ corresponds to one full migratory cycle within a year, and movement from $x = L$ back to $x = 0$ corresponds to the next full cycle. In other words, if in odd-numbered years the resource peak travels from $x = 0$ to $x = L$, then in even-numbered years it moves from $x = L$ to $x = 0$ in the folded 2D representation of Fig. 3 (b). Because periodic boundary conditions are imposed at $x = 0$ and $x = L$, plotting the population distribution on the reduced spatial interval $[0, L/2]$ is not straightforward. Therefore, we present the spatial domain as $[0, L]$ in the 2D plane. As a consequence, the memory window becomes $\tau = 2T = 730$ (see Table 2). This doubling of the environmental period arises from the fact that the direction of resource movement alternates between consecutive years on the folded 2D plane (one year from $x = 0$ to $x = L$, the next from $x = L$ to $x = 0$) even though these directions are indistinguishable in the true cylindrical geometry (i.e., in the real world), where $x = 0$ and $x = L$ denote the same location (see Fig. 3 (a)). The perceived landscape, $h(x, t)$, is a spatially smoothed version of the resource, representing the animal's imperfect nonlocal sensory perception. This

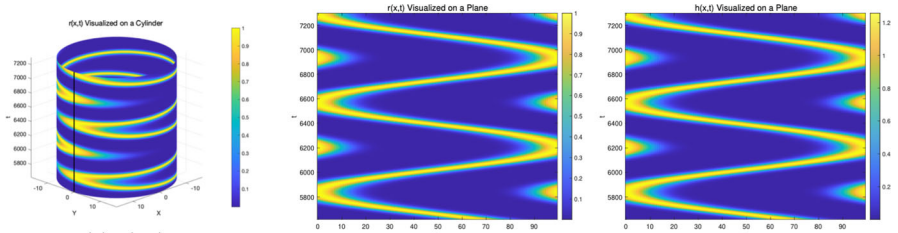

(a) r(x,t) (b) r(x,t) (c) h(x,t)

Fig. 3 The spatio-temporal dynamics of the prescribed resource $r(x, t)$ and the corresponding perceived resource landscape $h(x, t)$ under baseline parameters

dynamic environment serves as the stage upon which the different migratory strategies will be evaluated.

5.1 The interplay of cognitive strategies: perception vs. memory

Given the dynamic environment established above, how do the primary cognitive forces (perception and memory) interact to produce a successful migratory strategy? To answer this question, we deconstruct the roles of perception- and memory-guided navigation by analyzing both the spatio-temporal dynamics and the quantitative tracking efficiency of the system under four distinct scenarios. As established, the population's movement is driven by two taxis forces: one toward the perceived landscape $h(x, t)$ with strength α and the other toward the historical memory map $m(x, t)$ with strength γ. We analyze the outcomes when these forces act in isolation and in combination, examining four representative cases: (1) **No Cognition** ($\alpha = 0, \gamma = 0$); (2) **Perception-Only** ($\alpha = 5, \gamma = 0$); (3) **Memory-Only** ($\alpha = 0, \gamma = 5$); and (4) a **Hybrid Cognitive Strategy** ($\alpha = 5, \gamma = 3$).

The results for the **No Cognition** case are presented in Fig. 4, where we observe two distinct outcomes for the population and its memory. The population density, $u(x, t)$, converges to a spatio-temporally uniform steady state (Fig. 4 (b)), with $u \approx 0.01$ across the entire domain. This occurs because, in the absence of any taxis forces, the system is governed solely by diffusion, which eradicates any spatial structure and drives the population to a uniform distribution. Interestingly, the memory map, $m(x, t)$, does not become uniform. Instead, it settles into a stationary, wave-like pattern that reflects the long-term temporal average of the perceived resource at each spatial point (Fig. 4 (a)).

Biologically, this scenario depicts a population that is behaviorally inert to environmental cues, leading to a complete failure in resource tracking. The persistent mismatch between the uniformly distributed population and the concentrated, moving resource pulse would result in widespread starvation, representing a catastrophically unsuccessful strategy. The memory, in this case, acts merely as a passive "sediment" of past environmental conditions, rather than an active navigational tool.

In stark contrast, the **Perception-Only** strategy proves to be highly effective, as shown in Fig. 5. We observe that the population density, $u(x, t)$, forms a sharp and cohesive migratory wave that dynamically mirrors the spatio-temporal pattern of the

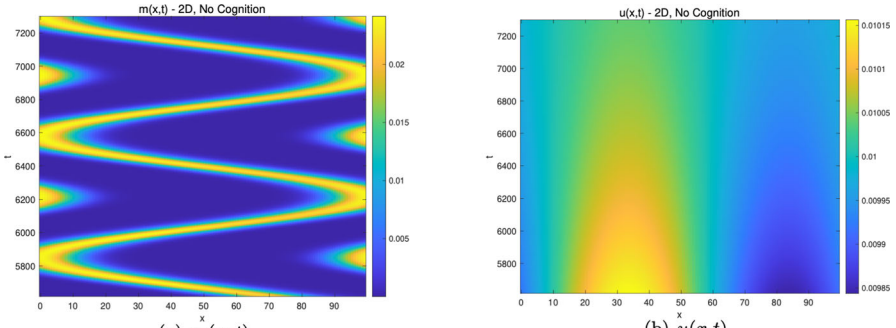

(a) $m(x,t)$ (b) $u(x.t)$

Fig. 4 Spatiotemporal dynamics for the No Cognition case ($\alpha = 0, \gamma = 0$). The population density converges to a uniform steady state, failing to track the perceived resource. The memory map settles into a stationary pattern reflecting the long-term average of the resource landscape, but does not guide the population

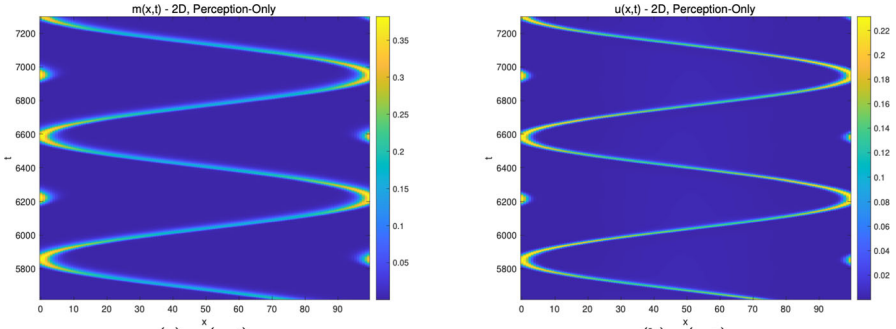

(a) $m(x,t)$ (b) $u(x,t)$

Fig. 5 Spatiotemporal dynamics for the Perception-Only case ($\alpha = 5, \gamma = 0$). The population successfully tracks the perceived resource, forming a cohesive migratory wave. The memory map is subsequently imprinted with this successful trajectory

resource landscape, $r(x,t)$ (Fig. 5 (b)). This successful tracking occurs because the movement is solely governed by a strong perception-driven taxis, which directs individuals to continually move up the gradient of the perceived resource. The population, therefore, acts as a reactive agent, skillfully "surfing" the wave of resource availability in real time.

A significant consequence is the effect on the memory map. As $m(x,t)$ is formed from the history of successful foraging, it is subsequently imprinted with this same successful migratory trajectory (Fig. 5 (a)). From an ecological perspective, this scenario represents an expert at immediate, sensory-based tracking. It demonstrates that a robust migratory route can be dynamically "learned" and encoded into a cognitive map purely through repeated sensory experience, without any pre-existing knowledge.

The **Memory-Only** strategy, presented in Fig. 6, also facilitates a successful migratory pattern, albeit with a distinct dynamic signature. We observe that the population forms a robust traveling wave guided by the trajectory encoded in the memory map. However, the population is not as strongly concentrated at the resource peaks as in the

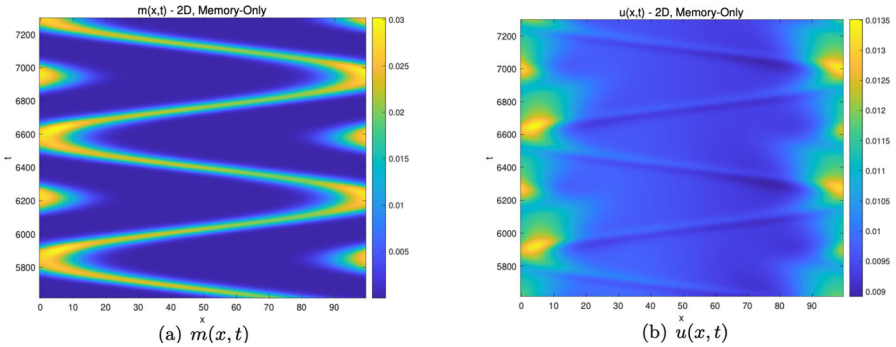

(a) $m(x,t)$ (b) $u(x,t)$

Fig. 6 Spatiotemporal dynamics for the Memory-Only case ($\alpha = 0, \gamma = 5$). Guided by a robust memory map, the population successfully establishes a migratory pattern, demonstrating the predictive power of long-term memory in a periodic environment

perception-only case. Instead, a substantial portion of the population also appears in regions without resource peaks.

This phenomenon arises because the population's movement is entirely proactive, driven solely by historical information. In our perfectly periodic environment, the memory map—an aggregation of past successful locations—serves as an accurate predictive tool, essentially a "navigational chart." This allows the population to anticipate the resource's path, a key advantage of memory-based navigation. From an ecological perspective, this represents a population guided by tradition or long-term experience.

Finally, the **Hybrid Cognitive Strategy**, shown in Fig. 7, demonstrates the synergistic effect of integrating both cognitive mechanisms. The population forms an exceptionally sharp and cohesive traveling wave, shaped by the combined influence of the reactive "pull" from perception and the proactive "guidance" from memory. This enhanced performance stems from the complementary nature of the two strategies: the strong perception component ensures precise, real-time tracking, while the memory component reinforces the overall migratory route, providing stability. This interplay, where memory provides the general path and perception offers fine-tuned adjustments, results in a sharply defined and stable memory map.

From an ecological viewpoint, this hybrid approach represents a more sophisticated form of navigation. It mirrors organisms that combine long-term knowledge (e.g., of seasonal routes) with immediate sensory information (e.g., of a food patch's current location). Such integration leads to a migratory behavior that is both highly efficient in its resource tracking and resilient to minor environmental fluctuations, arguably representing a more robust and evolutionarily advantageous strategy.

To quantitatively evaluate the movement efficiency of these distinct strategies, we computed the **Average Time Lag**. This metric is derived from a time-series cross-correlation analysis between the population's center of mass, $x_{\text{com}}(t)$, and the true resource center, $x_0(t)$. A positive lag indicates that the population follows the resource with a delay.

The simulation results for this analysis are presented in Fig. 8. The **Memory-Only Strategy** (Panel b) failed to generate a meaningful migratory pattern, resulting

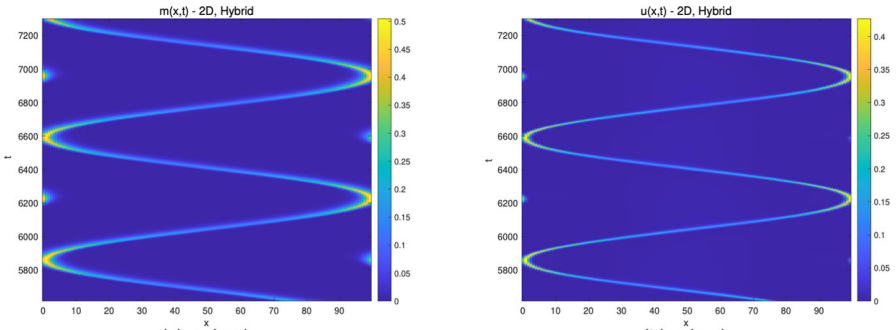

(a) $m(x,t)$ (b) $u(x,t)$

Fig. 7 Spatiotemporal dynamics for the Hybrid Strategy ($\alpha = 5, \gamma = 3$). The integration of strong perception and memory results in a highly efficient migratory pattern, with the population closely tracking the resource and forming a sharp, stable memory map

in a large and erratic lag. While the **Perception-Only Strategy** (Panel a) successfully tracked the resource movement, a significant delay is clearly observed, with the population's center of mass consistently lagging behind the resource center. In stark contrast, the **Hybrid Cognitive Strategy** (Panel c) exhibited a much closer alignment between the trajectories, demonstrating that combining memory and perception allows the population to respond in a far more coordinated and anticipatory manner. The bar graph (Panel d) quantitatively confirms this visual observation, showing that the Hybrid Cognitive Strategy markedly reduces the average time lag compared to the Perception-Only and Memory-Only Strategies, highlighting the adaptive advantage of integrating both cognitive tools.

To provide a comprehensive quantitative assessment and synthesize these findings, we computed the time-averaged Spatiotemporal Overlap ($\overline{\text{STO}}$) index across the entire α-γ parameter space. This metric, a Bhattacharyya-type overlap adapted from Fagan et al. (2022), measures the match between population and resource distributions. It is calculated by time-averaging the instantaneous spatial overlap, $\Omega_{\text{STO}}(t)$:

$$\overline{\text{STO}} = \frac{1}{T} \int_{t_{\text{end}}-T}^{t_{\text{end}}} \left(\frac{\int_\Omega \sqrt{u(x,t) r(x,t)}\, dx}{\sqrt{\int_\Omega u(x,t)\, dx} \sqrt{\int_\Omega r(x,t)\, dx}} \right) dt. \tag{5.1}$$

Values of $\overline{\text{STO}}$ near 1 indicate tight co-location, whereas values near 0 indicate poor matching.

Figure 9 reveals a sophisticated interplay between perception strength (α) and memory strength (γ) in driving migration efficiency. Contrary to the intuition that simultaneously maximizing both would yield the best performance, the landscape demonstrates that a strong α coupled with a strong γ does not produce the highest efficiency. The peak STO values are obtained when the perception strength is relatively small (around $\alpha = 1$) across variable memory strengths as well as when the population adopts perception-only strategy with a higher perception strength (near $\alpha = 5$).

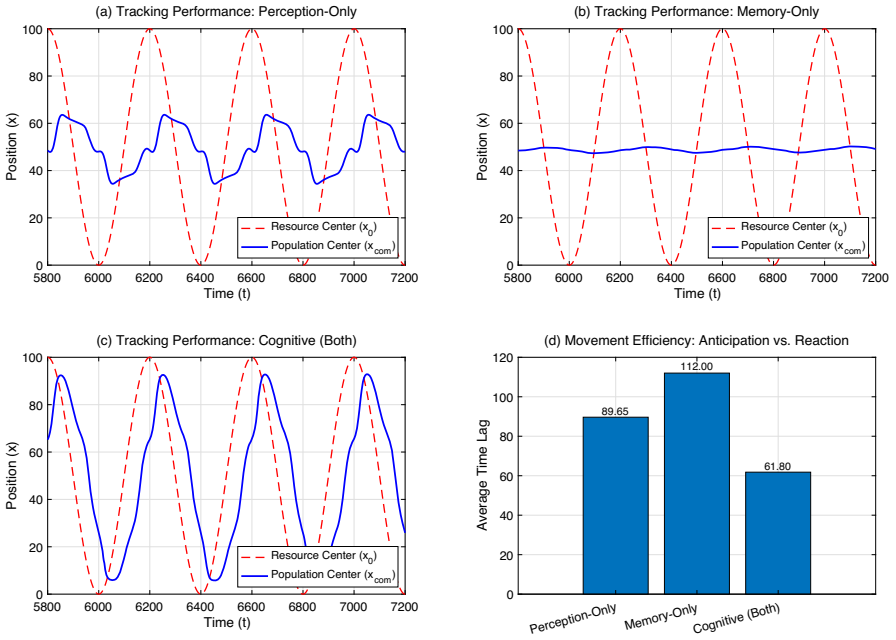

Fig. 8 This figure compares movement efficiency for three strategies: Perception-Only ($\alpha > 0$, $\gamma = 0$), Memory-Only ($\alpha = 0$, $\gamma > 0$), and Hybrid Cognitive ($\alpha, \gamma > 0$). Panels (a–c) show the population's center of mass (x_{com}, solid blue) vs. the true resource center (x_0, dashed red) from $t = 5800$ to $t = 7200$. Panel (d) presents the Average Time Lag from cross-correlation analysis. The Memory-Only Strategy fails to track the resource, while the Hybrid Cognitive Strategy markedly reduces lag compared to the Perception-Only Strategy, highlighting the advantage of combining memory with perception

5.2 The role of memory precision (ε)

Having examined the primary cognitive forces, we now investigate the influence of a more nuanced trait: memory precision. In our model, this is quantified by the memory diffusion parameter, ε, which controls the spatial specificity of the cognitive map. This parameter ranges from a highly accurate, point-like recall (low ε) to a highly generalized or "fuzzy" memory (high ε). The precision of spatial memory represents a fundamental cognitive trade-off: a hyper-precise memory may allow for exact relocation of known resources but could hinder adaptation to environmental shifts, while a memory that is too fuzzy may fail to provide any useful spatial guidance. This raises a key ecological question: Is there an optimal level of memory precision for tracking dynamic resources?

To address this question, we conducted a series of simulations designed to isolate the effect of ε while keeping all other parameters fixed at their baseline values (Table 2). We varied ε across several orders of magnitude and focus our analysis on three representative scenarios: a high- ($\varepsilon = 0.01$), an intermediate- ($\varepsilon = 0.2$), and a low-precision ($\varepsilon = 2.0$) case. To isolate the effects of memory on resource-tracking efficiency, we select parameter values that minimize the influence of perception—driven movement. Specifically, we set the perception-driven taxis strength to a small

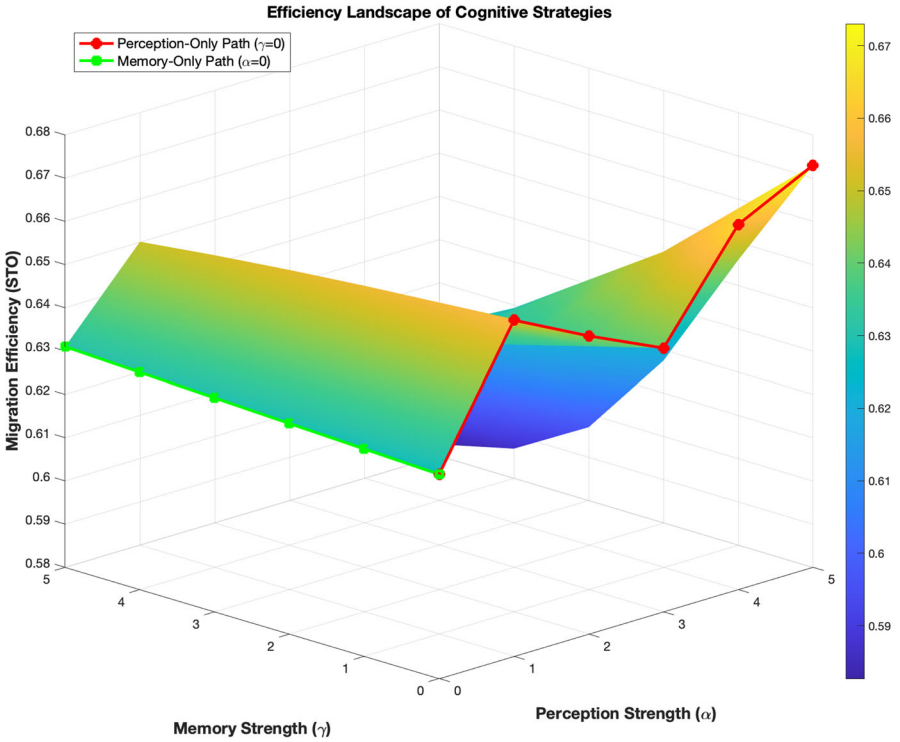

Fig. 9 Migration efficiency

value ($\alpha = 0.01$), ensuring that local sensory cues provide only a weak directional signal. In contrast, we choose a comparatively larger memory–driven taxis strength ($\gamma = 1$) so that movement guided by internal memory plays the dominant role. This parameter choice allows us to focus on how variations in memory precision shape the population's ability to locate and track resource peaks, without confounding effects from strong perception-based responses.

The simulation results, presented in Figs. 10 and 11, reveal a stark, threshold-dependent relationship between memory precision and migration success. Qualitatively, Fig. 10 illustrates a clear transition in behavior. For both high ($\varepsilon = 0.01$) and intermediate ($\varepsilon = 0.2$) precision, the memory map $m(x, t)$ successfully forms coherent spatio-temporal tracks, enabling the population $u(x, t)$ to form a cohesive migratory wave that effectively tracks the perceived resources (Fig. 10 (b) and (d)). The primary difference is that lower ε values lead to sharper, more concentrated population and memory peaks. However, a dramatic shift occurs at $\varepsilon = 2.0$ (Fig. 10 (f)). The strong diffusive effect completely eradicates the spatial structure of the memory map. Deprived of this cognitive guidance, the population fails to maintain a migratory pattern and collapses into a spatially uniform distribution, indicating a catastrophic failure of the strategy.

The quantitative analysis, presented in Fig. 11, confirms the qualitative findings from Fig. 10. The STO index exhibits a clear, monotonic decrease as the memory

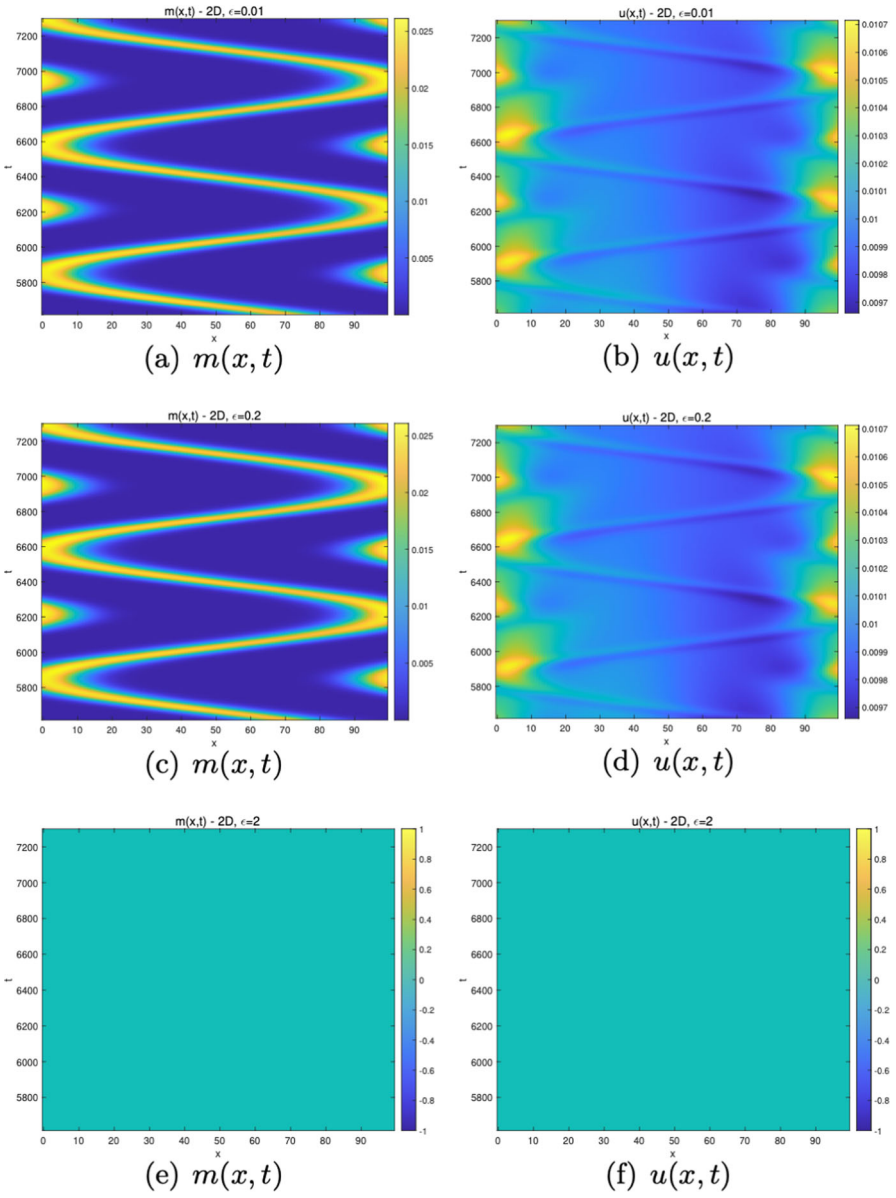

Fig. 10 Effect of memory diffusion (ε) on the spatio-temporal dynamics. Each row corresponds to a different value of ε: high-precision ($\varepsilon = 0.01$, top), intermediate ($\varepsilon = 0.2$, middle), and low-precision ($\varepsilon = 2.0$, bottom). For each case, 2D plots for the memory map $m(x,t)$ and population density $u(x,t)$ are shown. Here, $\alpha = 0.01$, $\gamma = 1$

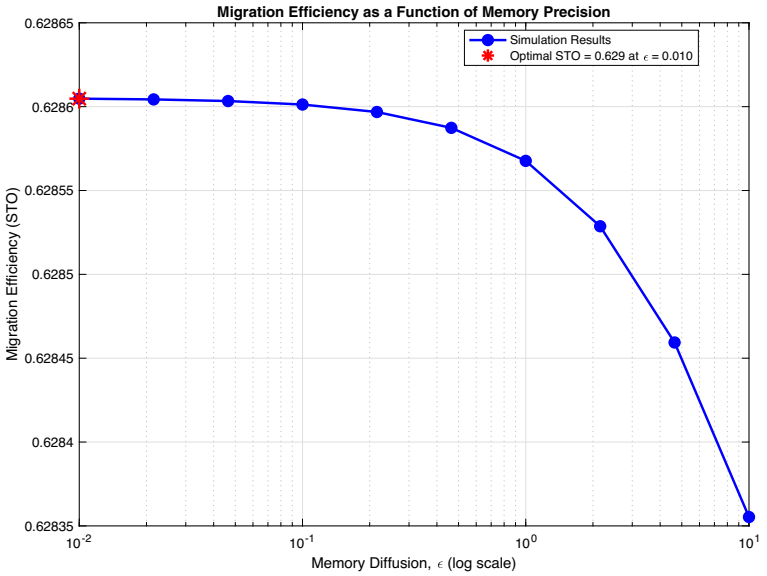

Fig. 11 Migration efficiency, measured by the Spatio-Temporal Overlap (STO) index, as a function of memory diffusion, ε (plotted on a log scale). Here, $\alpha = 0.01$, $\gamma = 1$

diffusion ε increases. This quantitatively demonstrates that a higher memory precision (lower ε) leads to a more effective migratory strategy, while a more diffuse memory (higher ε) degrades the population's ability to track the resource.

Ecologically, these findings highlight the importance of maintaining a sufficient level of cognitive precision for migration. A moderately generalized memory (e.g., $\varepsilon = 0.2$) is shown to be nearly as effective as a hyper-precise one (e.g., $\varepsilon = 0.01$), suggesting that a "good enough" memory system can be a cost-effective evolutionary strategy. However, as memory becomes excessively diffuse, the progressive decline in the STO score reflects a systematic failure of the navigational strategy. This underscores how gradual degradation in (collective) memory could lead to a corresponding decline in the success of large-scale animal migrations. For other types of models that explore this idea, see William F Fagan et al. (2012); Berdahl et al. (2018); Foss-Grant et al. (2018) and for relevant empirical studies see Brett R Jesmer et al. (2018); Werner T Flueck et al. (2022).

5.3 The role of the memory timescale (τ)

Having established the interplay between perception and memory, we now investigate a more fundamental question: how does the timescale of memory itself, governed by τ, shape the migratory strategy? We expect that the utility of a memory is contingent on its temporal alignment with the environment's periodicity. A memory mismatched with the environmental cycle could be detrimental, while a seasonally-matched memory could be highly beneficial. To explore this, we fixed the cognitive strengths to a

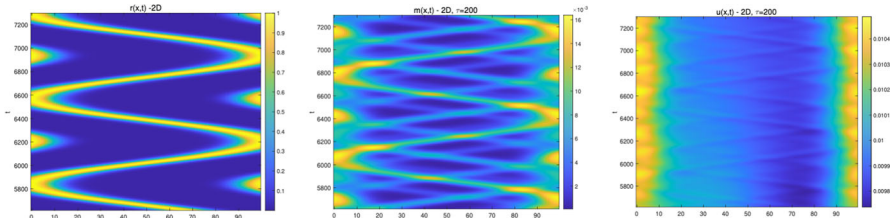

(a) $r(x,t)$ (b) $m(x,t)$, $\tau = 200$ (c) $u(x,t)$, $\tau = 200$

Fig. 12 System dynamics under a mismatched, anti-phasic memory window ($\tau = 200$). The memory map $m(x,t)$ becomes chaotic and disordered, as it is being fed conflicting information. The population distribution $u(x,t)$ does not match well with the resource distribution

memory-dominant regime ($\alpha = 0.01$, $\gamma = 1$) and presented two representative cases: a mismatched ($\tau = 200$) and a long-term seasonal ($\tau = 730$) memory.

First, it is important to clarify our model's temporal structure. We simulate population dynamics on a one-dimensional domain $[0, L]$ with periodic boundary conditions, which can be visualized as an "unrolled" circular habitat. The resource wave completes a full unidirectional circuit over a period of $T = 365$ days. When plotted on a 2D spatio-temporal graph, however, this single circuit appears as two distinct visual crossings. Therefore, for a memory to be perfectly synchronous with the visual pattern over cycles, a memory window of $\tau = 730$ is an appropriate choice.

The simulation results, presented in Figs. 12 and 13, reveal that the temporal scale of memory has a profound effect on the resulting dynamics. When the memory window length is set to be a long-term, seasonal timescale ($\tau = 730$, Fig. 13), we observe that the memory, synchronous with the environmental cycle, transforms into a powerful predictive tool. This is reflected in the population wave, which becomes visibly concentrated, with high peak amplitudes and a strong contrast between high and low-density regions, indicating an effective migratory strategy. However, the situation changes dramatically for a mismatched memory window ($\tau = 200$, Fig. 12). In this case, the memory map becomes highly disordered due to conflicting, nearly anti-phasic information. In our memory-dominant regime ($\gamma \gg \alpha$), this chaotic signal severely perturbs the system, causing the population to fail to form a coherent traveling wave. Instead, it exhibits a highly disturbed and unstable pattern, indicating a severely compromised migratory strategy. From an ecological standpoint, these findings demonstrate that a memory system's timescale must be finely tuned to the rhythms of the environment to be adaptive. A mismatched memory is not just useless; it is actively detrimental, severely disrupting the formation of a stable migratory pattern. Our results thus quantitatively confirm that the success of a cognitive strategy depends not just on the strength of its components, but critically on their temporal alignment with the ecological problem they have evolved to solve.

Mapping model regimes to ecological strategies. Our model reveals that distinct combinations of perception strength (α) and memory influence (γ) correspond to qualitatively different cognitive movement strategies. These parameter regimes can be conceptually linked to characteristic ecological archetypes (Table 3). When perception dominates (high α, low γ), movement is primarily reactive to instantaneous resource

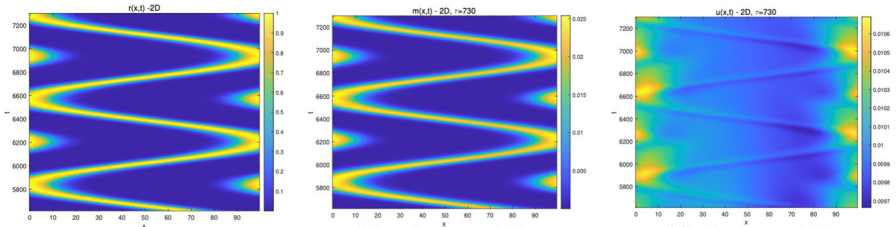

(a) $r(x,t)$ (b) $m(x,t)$, $\tau = 730$ (c) $u(x,t)$, $\tau = 730$

Fig. 13 System dynamics under a long-term, seasonal memory window ($\tau = 730$). The memory map $m(x,t)$ now forms a sharp, predictive trajectory that is perfectly in-phase with the resource landscape. The resulting population wave $u(x,t)$ is highly cohesive and efficient in resource tracking

cues, resembling the behavior of pelagic seabirds such as albatrosses that track transient oceanic fronts in highly unpredictable environments. In contrast, when memory dominates (high γ, low α), individuals rely on long-term spatial knowledge to revisit predictable resource landscapes, as seen in long-distance ungulates like mule deer that follow highly traditional migratory routes across seasons. Between these extremes lies an integrated strategy (high α, high γ), where both memory and perception jointly guide migration. This hybrid regime mirrors the behavior of cognitively advanced species such as elephants and whales, which combine stable, memory-based migratory corridors with flexible, real-time adjustments to local conditions. Altogether, this mapping illustrates how our theoretical framework captures a continuum of cognitive strategies–from reactive foraging to memory-based navigation–providing ecological context for the parameter-dependent migration patterns observed in our simulations.

6 Discussion

Seasonal migration is one of nature's most remarkable large-scale behaviors, driven by animals' need to exploit spatiotemporally varying resources and avoid unfavorable conditions. Increasing evidence shows that such migrations are not merely reactions to real-time environmental cues, but are instead guided by cognitive processes integrating perception and memory (Jerod et al. 2019; Bauer et al. 2020; Abrahms et al. 2019; Brett R Jesmer et al. 2018). Migratory species—from marine predators such as blue whales to terrestrial and avian migrants—often rely on past experiences to revisit historically resource-rich habitats, combining current sensory perception with stored information accumulated across years. This integration allows individuals to navigate cyclically changing environments efficiently, though it also introduces trade-offs between flexibility and reliability: perception enables rapid adaptation to current conditions, while memory provides long-term consistency but may be imperfect or outdated. Understanding how these mechanisms jointly drive migration has become essential not only for advancing cognitive movement ecology, but also for predicting species' responses to environmental change (Wilcove and Wikelski 2008; Gurarie et al. 2019; Kauffman et al. 2021; Gurarie et al. 2024). Existing theoretical and empirical studies have demonstrated the importance of nonlocal perception and memory

Table 3 Conceptual mapping of model parameter regimes to ecological strategies

Strategy Profile	Model Parameter Regime	Ecological Archetype
Reactive Forager (Perception-Dominant)	High α, Low γ,	*Pelagic Seabirds* (e.g., Albatrosses) tracking unpredictable oceanic fronts (Weimerskirch et al. 1993; Scales et al. 2017; Fauchald 1999)
Conservative Navigator (Memory-Dominant)	High γ, Low α,	*Long-route Ungulates* (e.g., Mule Deer) following highly traditional, predictable migratory circuits (Sawyer et al. 2005, 2009)
Integrated Navigator (Hybrid Cognitive Strategy)	High α, High γ,	*Long-lived Animals* (e.g., Elephants, Whales) using a traditional map but making real-time adjustments (Abrahms et al. 2019; Bracis and Mueller 2017; Polansky et al. 2015)

in guiding seasonal migration, yet a unified population-level PDE framework that dynamically couples perception, memory formation, and seasonally varying resource fields along with a complete analysis of its emergent dynamics has been lacking. Motivated by these gaps and inspired by recent findings on memory-based blue whale migration (Abrahms et al. 2019), our work develops and analyzes a novel PDE model that explicitly links nonlocal perception and evolving memory in a seasonally forced environment. This framework provides new insights into how the interaction between perception and memory shapes the emergence and stability of round-trip seasonal migrations, offering a theoretical foundation for understanding cognitive adaptation in a changing world.

Our modeling framework combines several behavioral processes central to seasonal migration. Diffusion captures undirected, random movement, reflecting baseline exploratory behavior. Perception-driven taxis allows individuals to respond to current resource distributions through nonlocal sensing, enabling rapid adjustments to shifting environments. Memory-driven taxis directs movement toward previously profitable locations, incorporating the influence of past experience. Our model further advances this approach by explicitly representing memory of seasonal resources through a sum of weighted coincidences between the population and resource availability over historical seasonal windows at each location. This novel formulation captures how animals accumulate and prioritize past experiences in temporally recurring landscapes, allowing us to investigate emergent trade-offs and distinct movement strategies under realistic seasonal and spatial dynamics. Building on this foundation, the model incorporates nonlocality in both perception-driven and memory-driven movement. Rather than responding only to resource levels at their immediate location, individuals assess resource availability over a spatial neighborhood through a nonlocal perception kernel, capturing realistic sensing ranges observed in many species. Importantly, this nonlocal structure also appears in the memory-driven taxis: memory is formed not from pointwise resource encounters, but from past nonlocal perceptions accumulated over historical seasonal windows. As a result, movement decisions are shaped by both current and remembered spatially distributed information, allowing the model to represent how animals integrate broad environmental cues across space and time. This dual nonlocal formulation leads to richer and more biologically grounded movement dynamics than purely local models, enabling the study of spatial anticipation, navigation efficiency, and emergent migration patterns in dynamic landscapes. Another distinctive feature of our model is a mathematically novel representation of fuzzy, or imprecise, memory by treating memory precision as a random diffusion term. This addition captures the idea that animals do not recall past experiences perfectly, and that the reliability of memory can fluctuate over time and space(Fagan et al. 2013; William F Fagan et al. 2023). Incorporating memory fidelity as an internal state adds a new layer of complexity to the PDE system, enabling the investigation of how uncertainty in stored information influences movement efficiency and emergent spatial patterns. This framework allows for a more realistic and mechanistic understanding of the interplay between cognitive limitations and adaptive migration strategies.

On the mathematical side, we established a complete set of fundamental properties for this model, including the global existence of solutions and, through the Leray-Schauder fixed-point theorem, the existence of at least one time-periodic solution.

These properties confirm that the model can sustain migratory patterns synchronized with seasonal forcing. In the mathematical analysis, our general approach follows the classical framework for analyzing PDEs, aimed at proving the existence, uniqueness, and stability of a periodic solution that represents a migratory pattern synchronized with the environment. The core methodologies included: first, establishing the global existence and well-posedness of solutions by obtaining key *a priori* L^∞-bounds through a detailed inductive argument, which overcomes the potential for solution blow-up caused by the taxis terms, followed by a continuation argument; second, proving the existence of periodic solutions using the Leray-Schauder fixed-point theorem in an appropriate Banach space; and finally, constructing a suitable Lyapunov-Krasovskii functional to establish sufficient conditions under which the periodic solution is unique and globally asymptotically stable. A cornerstone of our mathematical framework is the assumption of periodicity in both space and time. This assumption is not merely a convenience, but is fundamental to the analysis, as it is leveraged in several critical steps. Specifically, periodicity eliminates boundary terms in the energy estimates for stability proofs, ensures the invertibility of key parabolic operators for existence theory, and guarantees the compactness properties essential for applying topological degree methods. Crucially, our construction of a Lyapunov-Krasovskii functional established the conditions for the uniqueness and global asymptotic stability of this periodic solution. The mathematical requirement that the taxis strengths (α, γ) must not be excessively large is particularly significant. It reveals a central trade-off between the directed, aggregation-driven forces of taxis and the system's inherent dissipative effects. This suggests that while perception and memory are essential for migration, overly strong directed movement can destabilize the unique migratory pattern, potentially leading to more complex dynamics such as multistability. This raises the intriguing ecological possibility that, under identical environmental conditions, different migration routes could emerge depending on a population's history.

Numerically, we employed MATLAB to solve the system based on the Method of Lines (discrete). For spatial discretization, we used a high-precision pseudo-spectral method, where spatial derivatives and convolutions were computed efficiently using the Fast Fourier Transform (FFT), which is well-suited for the periodic domain. For time integration, the classical fourth-order Runge-Kutta (RK4) scheme was used. The main challenges in the numerical implementation were twofold. The first was ensuring the fidelity of the model's implementation, which was addressed by code review to correct initial misinterpretations of the kernel normalization and the memory formation term. The second challenge was maintaining numerical stability. We found that for large taxis strengths (α, γ), a relatively large time step violated a Courant-Friedrichs-Lewy (CFL)-like stability condition, leading to spurious numerical artifacts. To resolve this, a smaller time step (e.g., $dt = 0.01$) was ultimately chosen, which, despite increasing computational cost, was necessary to obtain reliable numerical results that faithfully represent the model's intrinsic dynamics. Our numerical explorations were designed to confirm the theoretical findings and to deconstruct the ecological implications of the core cognitive mechanisms. The simulations first visually verify the theoretical prediction of global convergence to a unique periodic attractor. A formal sensitivity analysis then quantitatively confirms that the taxis strengths, α and γ, are indeed the model's most critical parameters, justifying our focus on them. Our detailed

subsequent analyses of these cognitive parameters reveal a complex picture of trade-offs, adding crucial layers of ecological context to our theoretical framework. First, the analysis of the α-γ efficiency landscape shows that hybrid perception-memory strategy is the overwhelmingly dominant driver of success in resource tracking. Second, the investigation of memory precision reveals the existence of a critical cognitive threshold, beyond which a memory that is to “fuzzy" becomes useless and causes the migratory strategy to collapse. Finally, and perhaps most profoundly, our results demonstrate that the adaptive value of memory is critically determined by its temporal scale. A seasonally-matched memory acts as a powerful predictive tool, whereas a mismatched memory is catastrophically detrimental.

The conceptual mapping of parameter regimes to ecological strategies, as summarized in Table 3, highlights the practical value of our model as a versatile theoretical framework for investigating the continuum of cognitive migration strategies observed in nature. By tuning key parameters (such as the strength of perception-driven advection (α) and that of memory-driven advection (γ)), the model can be adapted to represent a wide range of migratory archetypes. For example, the Reactive Forager regime (high α, low γ) captures animals like albatrosses that rely on real-time perception of dynamic oceanographic features, while the Conservative Navigator regime (high γ, low α) reflects species such as mule deer that follow long-established migratory corridors. The Integrated Navigator profile (high α and γ) models the sophisticated plasticity of cognitively advanced species like elephants or blue whales, which combine spatial memory of traditional ranges with adaptive responses to real-time environmental cues. Beyond serving as a conceptual tool, our model provides a quantitative virtual laboratory for addressing pressing ecological and conservation questions. It can be used to assess how memory-dominant species might struggle to adapt under accelerating climate change, to identify the critical memory fidelity required for successful migration, or to evaluate the potential collapse of migratory culture following disruptions in social information transfer. Furthermore, by integrating empirical data—such as satellite tracking records for endangered species like blue whales—our framework can be parameterized and validated to characterize when, where, and how effectively animals track seasonal resource changes in increasingly resource-poor or shifting environments. In this way, the model provides one bridge between theory and data, offering a unified platform to explore the resilience, adaptability, and cognitive requirements of migration across diverse ecological contexts.

Although our model provides a unifying framework for studying cognitive migration, several limitations should be acknowledged. First, the model is built on a simplified one-dimensional resource landscape with perfectly periodic and predictable seasonal pulses. This abstraction facilitates mathematical analysis but does not capture the spatial heterogeneity and nonstationary dynamics of real ecosystems, where resource availability varies across complex terrains and shifts in response to climate change. Extending the model to higher-dimensional and interannually variable resource fields—whether through gradual climate-driven trends or stochastic fluctuations in timing and magnitude—would allow assessment of how robust the identified migratory strategies are when historical patterns no longer reliably predict future conditions.

Second, although our formulation includes dynamic memory, it aggregates diverse cognitive processes into a single memory field. In reality, animals integrate multiple memory types operating over different timescales. A promising avenue for future work is to incorporate short-term memory alongside the long-term seasonal memory represented here. Short-term memory influences fine-scale decisions such as stopover selection, path adjustment, and responses to unexpected environmental changes (see, e.g., Wang and Salmaniw (2023) for a discussion about long-term vs. short-term memory). A unified multiscale memory structure within the PDE framework would provide deeper insight into how animals balance recent perception with accumulated experience, and when memory enhances or undermines successful migration in variable environments.

Third, social and cultural processes are only implicitly represented in the population-level formulation. Many migratory species rely on leader–follower dynamics, social learning, or culturally transmitted routes, important topics that have been explored both theoretically and with animal movement data(Mueller 2013; Polansky et al. 2015; Ellen O Aikens et al. 2024; Foss-Grant et al. 2018; William F Fagan et al. 2012; Berdahl et al. 2018; Gurarie et al. 2021) Incorporating explicit social networks or cultural memory components would improve understanding of how collective decision-making stabilizes or destabilizes migration under environmental change.

Finally, our model isolates cognitive and spatial processes by omitting demographic dynamics, resource depletion, and multispecies interactions. Introducing reaction terms for birth and death, or coupling movement to resource consumption, would clarify how population persistence and movement strategies coevolve. Extending the framework to multi-species systems–for example, memory- and perception-based predator–prey or competitive interactions–could reveal how cognitive strategies shape coexistence, spatial segregation, and emergent community-level migration patterns (see, e.g., Shi et al. (2021); Song et al. (2022) for memory-based movement models with two species in non-seasonal environments).

Rapid environmental change–including accelerating climate trends and increasing anthropogenic disturbance–is reshaping the seasonal resource cycles that many migratory species have relied upon for generations. The ability of animals to adapt to these shifting conditions hinges strongly on their cognitive capacities, particularly the integration of current perception with imperfect and decaying memory. These processes are notoriously difficult to observe directly in the wild, underscoring the value of rigorous theoretical frameworks that can illuminate their ecological consequences. By developing and analyzing a mechanistic PDE model that couples nonlocal perception, dynamically evolving memory, and seasonally forced resource landscapes, we have provided both qualitative and quantitative insights into the conditions that support successful seasonal migration. We hope that these results offer a foundation for future empirical and theoretical work aimed at understanding the cognitive underpinnings of adaptability and resilience in a rapidly changing world.

Acknowledgements Q.A. acknowledges support from the National Natural Science Foundation of China (No. 12101318) and the Natural Science Foundation of Jiangsu province (No. BK20200805). X.W. acknowledges support from the U.S. National Science Foundation (NSF LEAPS-MPS 2532311). P.B. acknowledges support from The Scientific and Technological Research Council of Türkiye (TÜBİTAK) under the 2219 Postdoctoral Research Fellowship Program (No. 1059B192402311). W.F. acknowledges support from the

U.S. National Science Foundation (DMS2451241). P.W. acknowledges support from the National Natural Science Foundation of China (No. 12201557) and the Fundamental Research Funds for the Provincial Universities of Zhejiang (No. GK249909299001-020). B.A. acknowledges support from the Alfred P. Sloan Foundation and David & Lucille Packard Foundation. H.W. acknowledges support from the Natural Sciences and Engineering Research Council of Canada (Individual Discovery Grant RGPIN-2025-05734) and a Canada Research Chair.

Data Availability No data were used in this study.

Declarations

Conflicts of Interest The authors declare that they have no conflict of interests.

References

Abrahms B, Hazen EL, Aikens EO, Savoca MS, Goldbogen JA, Bograd SJ, Jacox MG, Irvine LM, Palacios DM, Mate BR (2019) Memory and resource tracking drive blue whale migrations. Proc Natl Acad Sci 116(12):5582–5587

Aikens EO, Kauffman MJ, Merkle JA, Dwinnell SPH, Fralick GL, Monteith KL (2017) The greenscape shapes surfing of resource waves in a large migratory herbivore. Ecol Lett 20(6):741–750

Aikens EO, Nourani E, Fiedler W, Wikelski M, Flack A (2024) Learning shapes the development of migratory behavior. Proc Natl Acad Sci 121(12):e2306389121

Alcázar-Treviño J, Johnson M, Arranz P, Warren VE, Pérez-González CJ, Marques T, Madsen PT, Aguilar N, de Soto. (2021) Deep-diving beaked whales dive together but forage apart. Proceedings of the Royal Society B Biological Sciences 288(1942):20201905

Alerstam T, Hedenström A, Åkesson S (2003) Long-distance migration: evolution and determinants. Oikos 103(2):247–260

Avgar T, Street G, Fryxell JM (2014) On the adaptive benefits of mammal migration. Can J Zool 92(6):481–490

Bailey H, Mate BR, Palacios DM, Irvine L, Bograd SJ, Costa DP (2009) Behavioural estimation of blue whale movements in the northeast Pacific from state-space model analysis of satellite tracks. Endangered Species Research 10:93–106

Ballance LT, Pitman RL, Fiedler PC (2006) Oceanographic influences on seabirds and cetaceans of the eastern tropical Pacific: A review. Prog Oceanogr 69:360–390

Bauer S, McNamara JM, Barta Z (2020) Environmental variability, reliability of information and the timing of migration. Proceedings of the Royal Society B Biological Sciences 287:20200622

Bell WJ (1991) Searching Behaviour: The Behavioural Ecology of Finding Resources. Chapman and Hall,

Berdahl AM, Kao AB, Flack A, Westley PAH, Codling EA, Couzin ID, Dell AI, Biro D (2018) Collective animal navigation and migratory culture: from theoretical models to empirical evidence. Philosophical Transactions of the Royal Society B Biological Sciences 373(1746):20170009

Bracis C, Mueller T (2017) Memory, not just perception, plays an important role in terrestrial mammalian migration. Proceedings of the Royal Society B Biological Sciences 284:20170449

Bradshaw WE, Holzapfel CM (2010) Light, time, and the physiology of biotic response to rapid climate change in animals. Annu Rev Physiol 72:147–166

José A, Carrillo Y, Salmaniw J, Skrzeczkowski (2024) Well-posedness of aggregation-diffusion systems with irregular kernels. arXiv preprint arXiv:2406.09227

Codling EA, Plank MJ, Benhamou S (2008) Random walk models in biology. J R Soc Interface 5:813–834

Dingle H (2014) Migration: The Biology of Life on the Move. Oxford University Press, 2nd edition

Dodson S, Oestreich WK, Savoca MS, Hazen EL, Bograd SJ, Ryan JP, Fiechter J, Abrahms B (2024) Long-distance communication can enable collective migration in a dynamic seascape. Sci Rep 14:14857

Fagan WF (2019) Migrating whales depend on memory to exploit reliable resources. Proc Natl Acad Sci 116(12):5217–5219

Fagan WF, Cantrell RS, Cosner C, Mueller T, Noble AE (2012) Leadership, social learning, and the maintenance (or collapse) of migratory populations. Thyroid Res 5(2):253–264

Fagan WF, Gurarie E, Bewick S, Howard A, Cantrell RS, Cosner C (2017) Perceptual ranges, information gathering, and foraging success in dynamic landscapes. Am Nat 189(5):474–489

Fagan WF, Lewis MA, Auger-Méthé M, Avgar T, Benhamou S, Breed G, LaDage L, Schlägel UE, Tang W, Papastamatiou YP, Forester J, Mueller T (2013) Spatial memory and animal movement. Ecol Lett 16(10):1316–1329

Fagan WF, McBride F, Koralov L (2023) Reinforced diffusions as models of memory-mediated animal movement. J R Soc Interface 20(200):20220700

Fagan WF, Saborio C, Hoffman TD, Gurarie E, Cantrell RS, Cosner C (2022) What's in a resource gradient? Comparing alternative cues for foraging in dynamic environments via movement, perception, and memory. Thyroid Res 15:267–282

Fauchald P (1999) Foraging in a hierarchical patch system. Am Nat 153:603–613

Flueck WT, Jo Anne M, Smith-Flueck ME, Escobar MZ, Fuchs B, Geist V, Heffelfinger JR, Black-Decima P, Gizejewski Z, Vidal F et al (2022) Loss of migratory traditions makes the endangered patagonian huemul deer a year-round refugee in its summer habitat. Conservation 2(2):322–348

Foss-Grant A, Bewick S, Fagan WF (2018) Social transmission of migratory knowledge: quantifying the risk of losing migratory behavior. Thyroid Res 11(3):257–270

Friedman A (1964) Partial Differential Equations of Parabolic Type. Prentice-Hall,

Gurarie E, Avgar T (2024) Editorial: Cognitive movement ecology. Front Ecol Evol 12:1360427

Gurarie E, Beaupré C, Couriot O, Cameron MD, Fagan WF, Joly K (2024) Evidence for an adaptive, large-scale range shift in a long-distance terrestrial migrant. Glob Change Biol 30(11):e17589

Gurarie E, Hebblewhite M, Joly K, Kelly AP, Adamczewski J, Davidson SC, Davison T, Gunn A, Suitor MJ, Fagan WF et al (2019) Tactical departures and strategic arrivals: Divergent effects of climate and weather on caribou spring migrations. Ecosphere 10(12):e02971

Gurarie E, Potluri S, Cosner GC, Cantrell RS, Fagan WF (2021) Memories of migrations past: sociality and cognition in dynamic, seasonal environments. Front Ecol Evol 9:742920

Hale JK (1977) Theory of Functional Differential Equations, vol 3. Applied Mathematical Sciences. Springer-Verlag, New York-Heidelberg

Hessing S, Risser N, Pichot L, Oudejans MG, Guilpin M, Barcelos LMD, Curé C, Visser F (2024) Context-driven communication during deep-sea foraging in a social toothed whale. Royal Society Open Science 11:240558

Irvine LM, Mate BR, Winsor MH, Palacios DM, Bograd SJ, Costa DP, Bailey H (2014) Spatial and temporal occurrence of blue whales off the U.S. west coast, with implications for management. PLoS ONE 9:e102959

Jesmer BR, Merkle JA, Goheen JR, Aikens EO, Beck JL, Courtemanch AB, Hurley MA, McWhirter DE, Miyasaki HM, Monteith KL et al (2018) Is ungulate migration culturally transmitted? evidence of social learning from translocated animals. Science 361(6406):1023–1025

Kauffman MJ, Cagnacci F, Chamaillé-Jammes S et al (2021) Mapping out a future for ungulate migrations. Science 372(6542):566–569

Ladyzhenskaya OA, Solonnikov VA, Ural'tseva NN (1968) Linear and Quasi-linear Equations of Parabolic Type, volume 23 of Translations of Mathematical Monographs. American Mathematical Society

Sleeman BD, Levine HA (1997) A system of reaction diffusion equations arising in the theory of reinforced random walks. SIAM J Appl Math 57(3):683–730

Lin HY, Fagan WF, Jabin PE (2021) Memory-driven movement model for periodic migrations. J Theor Biol 508:110486

Martínez-García R, Calabrese JM, Mueller T, Olson KA, López C (2013) Optimizing the search for resources by sharing information: Mongolian gazelles as a case study. Phys Rev Lett 110(24):248106

Mate BR, Lagerquist BA, Calambokidis J (1999) Movements of north pacific blue whales during the feeding season off southern California and their southern fall migration. Mar Mamm Sci 15:1246–1257

Merkle JA, Monteith KL, Aikens EO, Hayes MM, Hersey KR, Middleton AD, Oates BA, Sawyer H, Scurlock BM, Kauffman MJ (2016) Large herbivores surf waves of green-up during spring. Proceedings of the Royal Society B Biological Sciences 283(1830):20160456

Merkle JA, Sawyer H, Monteith KL, Dwinnell SP, Fralick GL, Kauffman MJ (2019) Spatial memory shapes migration and its benefits: evidence from a large herbivore. Ecol Lett 22:1797–1805

Milner-Gulland EJ, Fryxell JM, Sinclair AR, (eds) (2011) Animal Migration: A Synthesis. Oxford University Press

Mueller T, Fagan WF (2008) Search and navigation in dynamic environments-from individual behaviors to population distributions. Oikos 117(5):654–664

Mueller T (2013) Robert B O'Hara, Sarah J Converse, Richard P Urbanek, and William F Fagan. Social learning of migratory performance Science 341(6149):999–1002
Murray JD (2002) Mathematical Biology I: An Introduction. Springer,(3rd edition)
Othmer HG, Stevens A (1997) Aggregation, blowup, and collapse: the ABC's of taxis in reinforced random walks. SIAM J Appl Math 57(4):1044–1081
Polansky L, Kilian W, Wittemyer G (2015) Elucidating the significance of spatial memory on movement decisions by African savannah elephants using state-space models. Proc R Soc B 282:20143042
Potts JR, Lewis MA (2019) Spatial memory and taxis-driven pattern formation in model ecosystems. Bull Math Biol 81:2725–2747
Sawyer H, Kauffman MJ, Nielson RM, Horne JS (2009) Identifying and prioritizing ungulate migration routes for landscape-level conservation. Ecol Appl 19(8):2016–2025
Sawyer H, Lindzey F, McWhirter D (2005) Mule deer and pronghorn migration in western wyoming. Wildl Soc Bull 33(4):1266–1273
Scales KL, Hazen EL, Jacox MG, Edwards CA, Boustany AM, Oliver MJ, Bograd SJ (2017) Scale of inference: on the sensitivity of habitat models for wide-ranging marine predators to the resolution of environmental data. Ecography 40(1):210–220
Shankar KH, Howard MW (2013) Optimally fuzzy temporal memory. J Mach Learn Res 14(1):3785–3812
Shi J, Wang C, Wang H (2019) Diffusive spatial movement with memory and maturation delays. Nonlinearity 32(8):3188–3208
Shi J, Wang C, Wang H (2021) Spatial movement with diffusion and memory-based self-diffusion and cross-diffusion. J Differential Equations 305:242–269
Shi J, Wang C, Wang H, Yan X (2020) Diffusive spatial movement with memory. J Dyn Diff Equat 32:979–1002
Smith HL (2011) An Introduction to Delay Differential Equations with Applications to the Life Sciences, vol 57. Texts in Applied Mathematics. Springer, New York
Somveille M, Manica A, Butchart SHM, Rodrigues ASL (2013) Mapping global diversity patterns for migratory birds. PLoS ONE 8(8):e70907
Song Y, Shi J, Wang H (2022) Spatiotemporal dynamics of a diffusive consumer-resource model with explicit spatial memory. Stud Appl Math 148(1):373–395
Song Y, Shuhao W, Wang H (2019) Spatiotemporal dynamics in the single population model with memory-based diffusion and nonlocal effect. J Differential Equations 267(11):6316–6351
Thompson PR, Derocher AE, Edwards MA, Lewis MA (2022) Detecting seasonal episodic-like spatio-temporal memory patterns using animal movement modelling. Methods Ecol Evol 13(1):105–120
Turchin P (1998) Quantitative Analysis of Movement: Measuring and Modeling Population Redistribution in Animals and Plants. Sinauer Associates,
Wang H, Salmaniw Y (2023) Open problems in PDE models for knowledge-based animal movement via nonlocal perception and cognitive mapping. J Math Biol 86(5):71
Weimerskirch H, Salamolard M, Sarrazin F, Jouventin P (1993) Foraging strategy of wandering albatrosses through the breeding season: A study using satellite telemetry. Auk 110(2):325–342
Wilcove DS, Wikelski M (2008) Going, going, gone: Is animal migration disappearing? PLoS Biol 6(7):e188
Jianhong W (1996) Theory and Applications of Partial Functional Differential Equations, vol 119. Applied Mathematical Sciences. Springer-Verlag, New York